GEO 610: Master Thesis

Combining Imaging Spectroscopy, Digital Object Models, and 3D Canopy Modelling to Advance Retrievals of Vegetation Information over Forest Ecosystems

Remote Sensing Laboratories
Department of Geography
University of Zurich

Master Thesis July 31, 2016

Author: Dominic Fawcett
Matriculation-Nr: 11-739-422
E-Mail: fawcettdominic@gmail.com

Faculty Representative: Prof. Dr. Michael E. Schaepman
Supervisor: Dr. Alexander Damm

Abstract

Employing imaging spectroscopy techniques in vegetation analysis offers unique capabilities for assessing functional traits of plants. However, illumination effects challenge the retrieval of vegetation information from high spatial resolution airborne or satellite data in areas of complex topography. Accurate pixel-wise descriptions of direct and diffuse irradiance components are necessary to perform an atmospheric correction that yields representative surface reflectances. These irradiance components are determined by the atmosphere as well as illumination-observation-surface geometry. We evaluate three atmospheric correction strategies that differ in their complexity to simulate actual and pixel-wise fractions of diffuse and direct irradiances. All approaches are physically-based and use either bulk digital elevation models (DEM), fine resolution digital object models (DOM), or 3D modelling outputs from the Discrete Anisotropic Radiative Transfer (DART) model. By calculating accurate top-of-canopy reflectances for the Laegern test-site in Switzerland, we seek to improve retrievals of the Normalized Difference Vegetation Index (NDVI), the Photochemical Reflectance Index (PRI) as well as relative contents of chlorophyll and carotenoids. We demonstrate that both the DOM and the DART based approach improve the retrieval of above indices for flat cast-shadows by 15.3-71.1% compared to the simple DEM case. Over a dense forest area, improvements are less clear. Remaining issues are mainly overestimations of resulting surface reflectances and retrieved indices due to extreme illumination conditions. We expect these issues to be partly resolved if higher resolution auxiliary data and more precise irradiance simulations are used, which however largely increases processing time. Going forward we also emphasize the potential of vegetation information retrieval from at-sensor radiances as a more efficient and robust solution.

Zusammenfassung

Die Anwendung von Bildspektrometrie zur Analyse von Vegetation bietet einzigartige Möglichkeiten, um die funktionalen Eigenschaften von Pflanzen zu bestimmen. Beleuchtungseffekte stellen jedoch hohe Herausforderungen an die Gewinnung von Vegetationsinformation aus Luft- und Satellitenbilddaten mit hoher räumlicher Auflösung in Gebieten mit komplexer Topographie. Genaue pixelweise Beschreibungen von direkten und diffusen Einstrahlungskomponenten sind nötig, um eine Atmosphärenkorrektur durchzuführen, welche repräsentative Oberflächenreflektanzen liefert. Diese Einstrahlungskomponenten werden von der Atmosphäre sowie von der geometrischen Konfiguration von Beleuchtung, Beobachter und Oberfläche bestimmt. Wir werten drei Strategien zur Atmosphärenkorrektur aus, die sich in der Komplexität ihrer Simulation von tatsächlichen, pixelweisen Anteilen von direkter und diffuser Einstrahlung unterscheiden. Alle Ansätze sind physikalisch basiert und benutzen entweder simple digitale Höhenmodelle (DEM), hoch aufgelöste digitale Objektmodelle (DOM) oder Outputs von 3D Modellierungen mit dem diskreten anisotropischen Strahlungstransfermodell (DART). Durch Berechnung von präzisen top-of-canopy Reflektanzen für das Lägern-Testgebiet in der Schweiz streben wir eine verbesserte Ableitung des "Normalized Difference Vegetation Index" (NDVI), des "Photochemical Reflectance Index" (PRI) sowie der relativen Gehalte von Chlorophyll und Carotenoiden an. Wir demonstrieren, dass sowohl der DOM als auch der DART basierte Ansatz die Bestimmung der oben genannten Indizes für flache Schlagschatten gegenüber dem einfachen DEM Ansatzes um 15.3-71.1% verbessern können. Über einem dicht bewaldeten Gebiet sind Verbesserungen nicht so eindeutig. Verbleibende Probleme sind Überschätzungen der Oberflächenreflektanzen und von abgeleiteten Indizes aufgrund extremer Beleuchtungssituationen. Wir erwarten, dass diese Probleme zum Teil durch höher aufgelöste Zusatzdaten und genauere Einstrahlungssimulationen gelöst werden können, was die Berechnungszeit jedoch enorm verlängern würde. Vorausblickend betonen wir das Potential von Methoden, die Vegetationsinformation aus Strahldichten am Sensor ableiten können, da diese eine effizientere und robustere Lösung anbieten.

Table of Contents

List of Figures

List of Tables

List of Nomenclature and Abbreviations

E_s^o ..... extra-terrestrial solar irradiance

E^{dif} ..... diffuse irradiance on a flat surface

E^{dir} ..... direct irradiance on a flat surface

E_{incl}^{dif} ..... diffuse irradiance on an inclined surface

K_{dif} ..... DART based scaling factor for diffuse irradiance

K_{Hay} ..... Hay's model scaling factor for diffuse irradiance

K_{dir} ..... DART based scaling factor for direct irradiance

L_{TOA} ..... radiance at top of atmosphere

φ_t ..... terrain slope azimuth angle

φ_s ..... solar azimuth angle

r ..... reflectance factor of the target

$\overline{r}$ ..... reflectance factor of the surroundings

r_{so} ..... bi-directional reflectance factor of the target

r_{do} ..... hemispheric-directional reflectance factor of the target

$\overline{r_{sd}}$ ..... smoothed directional-hemispherical reflectance factor of the surroundings

$\overline{r_{dd}}$ ..... smoothed bi-hemispherical reflectance factor of the surroundings

ρ_{so} ..... atmospheric bi-directional reflectance

ρ_{dd} ..... spherical albedo at the bottom of the atmosphere

SIF_s ..... emitted sun-induced chlorophyll fluorescence radiance of the target in observer-direction

SIF_d ..... hemispherical fluorescence flux of the surroundings

τ_{ss} ..... direct atmospheric transmittance in sun-direction

τ_{oo} ..... direct atmospheric transmittance in view-direction

τ_{sd} ..... diffuse atmospheric transmittance for the solar incidence
τ_{do} ..... directional atmospheric transmittance for diffuse incidence
θ_{il} ..... illumination zenith angle
θ_s ..... local solar zenith angle
θ_t ..... terrain slope inclination angle
V_{sun} ..... viewing factor for direct irradiance
V_{sky} ..... viewing factor for diffuse irradiance
2D ..... Two-dimensional
3D ..... Three-dimensional
a.s.l. ..... above sea level
AERONET .... AErosol RObotic NETwork
ALS ..... Airborne Laser Scanning
AOT ..... Aerosol Optical Thickness
APEX ..... Airborne Prism EXperiment
ATCOR ..... Atmospheric and Topographic CORrection
BHRF ..... Bi-Hemispherical Reflectance Factor
BOA ..... Bottom Of Atmosphere
BRF ..... Bi-directional Reflectance Factor
CAR ..... relative CARotenoid content index
CHL ..... relative CHLorophyll content index
DART ..... Discrete Anisotropic Radiative Transfer
DEM ..... Digital Elevation Model
DGVM ..... Dynamic Global Vegetation Model
DHM25 ..... Digital Height Model with 25m resolution
DHRF ..... Directional-Hemispherical Reflectance Factor
DOM ..... Digital Object Model
ESA ..... European Space Agency
FLEX ..... FLuorescence EXplorer
GPP ..... Gross Primary Production
HCRF ..... Hemispherical-Conical Reflectance Factor
HDRF ..... Hemispherical-Directional Reflectance Factor
IFOV ..... Instantaneous Field Of View
IRC ..... Integrated Radiometric Correction

IS ..... Imaging Spectroscopy
LiDAR ..... Light Detection And Ranging
LUE ..... Light Use Efficiency
LUT ..... Look-Up Table
MCMC ..... Monte Carlo Markov Chains
MODTRAN ... MODerate resolution atmospheric TRANsmission
NDVI ..... Normalized Difference Vegetation Index
NIR ..... Near InfraRed
NPQ ..... Non-Photochemical Quenching
PAI ..... Plant Area Index
PARGE ..... PARametric GEocoding
PRI ..... Photochemical Reflectance Index
RGB ..... Red-Green-Blue
ROI ..... Region Of Interest
RS ..... Remote Sensing
SCOPE ..... Soil Canopy Observation, Photochemistry, and Energy fluxes
SIF ..... Solar Induced Fluorescence
SLC ..... Soil-Leaf-Canopy
TOA ..... Top-Of-Atmosphere
TOC ..... Top-Of-Canopy
UAV ..... Unmanned Aerial Vehicle

1 | Introduction

Monitoring the dynamics of our planet's biosphere is key to ensure a timely identification of changes. These can range from large or global scale, like shifts in phenology (Cleland et al., 2007), to small scale changes such as crops experiencing water stress (Tilling et al., 2007). Information on these phenomena allows appropriate reactions and adaptation of future strategies (e.g. McVicar & Jupp, 1998). In order to make monitoring efficient and improve coverage, remote sensing (RS) has become the tool of choice, available at a variety of scales through UAV, aircraft, or satellite platforms (e.g. Berni et al., 2009; Kustas & Norman, 1996). Retrieving properties of the Earth's surface from RS measurements has however proven to be challenging. Especially in imaging spectroscopy (IS), a passive RS technique, there are a large number of undesired influences contributing to the retrieved signal. A multitude of absorption and scattering effects inhibit the path of electromagnetic radiation through the Earth's atmosphere. These must be removed by converting radiance to surface reflectance values. Early solutions sought to remove atmospheric effects using empirical methods, relying on scene specific information which meant that resulting relative reflectance values of two different scenes were not necessarily comparable (e.g. Conel et al., 1987; Kruse, 1988; Roberts et al., 1986). In the 1990s there was a push towards physically based atmospheric correction approaches, simulating the propagation of radiation within the atmosphere using radiative transfer codes such as MODTRAN (Berk et al., 1989) along with basic topographic models of the Earth's surface. With IS sensor spatial resolution increasing, describing radiative transfer becomes even more challenging as it is now heavily influenced by small scale topography. Simply using a digital terrain model (DTM) of the Earth's surface in the radiative transfer to describe irradiance, as is common practice (e.g. Richter, 1998), is not sufficient in these cases. This is relevant if a scene contains larger vegetation canopies like trees and if the illumination conditions lead to cast-shadows.

Errors in the assumption of irradiance composition, meaning the fractions of direct and

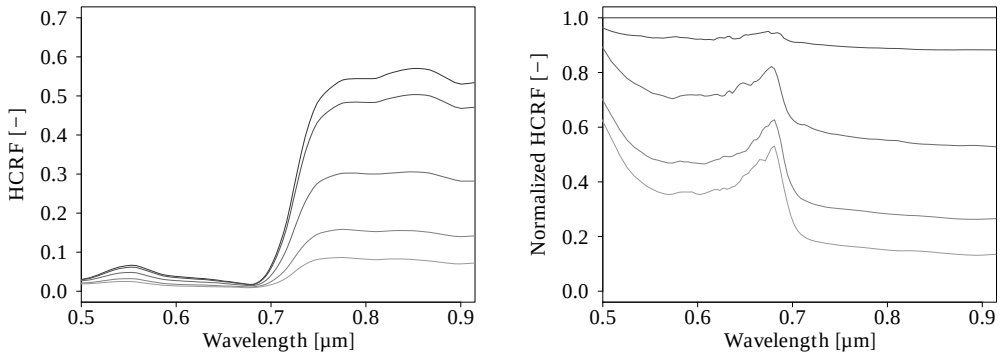

Figure 1.1.: TOC HCRF resulting from ATCOR, along a gradient from fully illuminated to cast-shadow (left) and the same reflectances normalized with the fully illuminated case (right).

diffuse radiation, have detrimental effects on atmospheric correction and the retrieved reflectance. This is illustrated in fig. (1.1) which shows the wavelength dependent effects introduced by assuming the same irradiance for surfaces receiving varying direct and diffuse contributions. Due to the effects visible in the top-of-canopy (TOC) reflectance normalized with the 100% direct irradiance case, retrieved vegetation indices based on ratios of reflectance at different wavelengths will exhibit illumination based variability. Cast-shadows are of course an extreme example but different illumination conditions can also be shown to have significant effects on vegetation variable retrieval over larger parts of a scene. Forests are the most susceptible, exhibiting large reflectance changes with variations of the solar zenith angle, if atmospheric compensation neglects the complex forest structure influencing irradiance. In an example of how this influences large scale statistics, indices for chlorophyll content (CHL) and carotenoid content (CAR) were computed from APEX data for the Laegern scene (courtesy of F. D. Schneider, UZH) containing sloped forested areas for two different times of day. As is clearly visible in the pigment maps of fig. (1.2) and the scatterplots of fig. (1.3), there is a shift in values of the two indices which is unlikely to be due to physiological changes and can be attributed to reflectance retrieval errors caused by wrong irradiance assumptions. Considering the subset used for fig. (1.3), the mean values for the indices deviate by 16.9% between the acquisition times for CHL and by 27.2% for CAR. Finding approaches to compensate this effect is therefore desirable.

This thesis consists of a study supplied in the form of a paper as will be submitted to

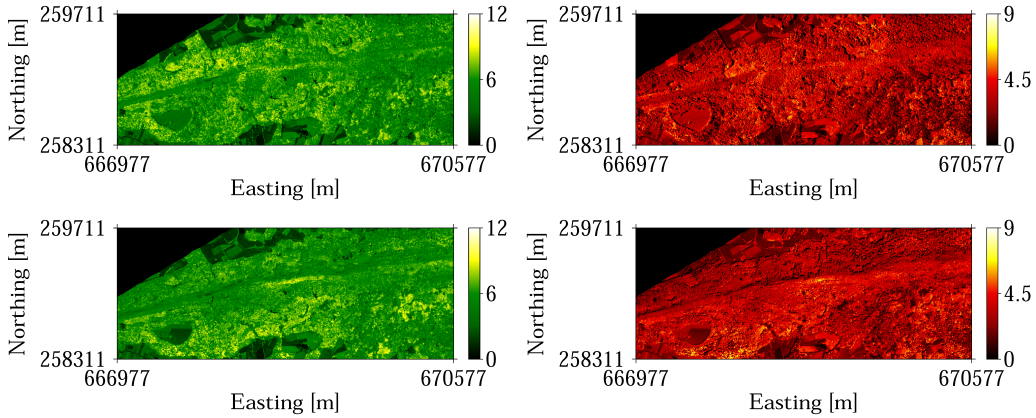

Figure 1.2.: Maps of chlorophyll (left, green) and carotenoid (right, red) index values of a scene subset for two different acquisition dates and times. Top: 26.06.2010 at 15:30 UTC, Bottom: 29.06.2010 at 10:00 UTC, Coordinates: CH1903 / LV03 (data courtesy of F. D. Schneider, UZH).

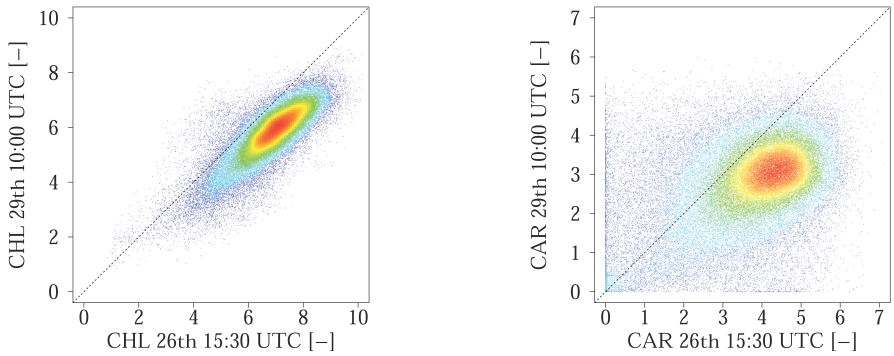

Figure 1.3.: Scatterplots of chlorophyll (left) and carotenoid (right) index values of a forest subset for two different acquisition dates and times (26.06.2010 at 15:30 UTC, 29.06.2010 at 10:00 UTC).

a major publisher. Aims of this study are to: i) develop a simple atmospheric correction procedure that yields results comparable to state of the art atmospheric correction software, ii) develop two approaches employing auxiliary data to more accurately describe irradiance on a per-pixel basis, the first employing a digital object model (DOM) and the second using scaling factors resulting from ray-tracing on a parameterized voxel-grid of the scene, and iii) compare and evaluate the approaches based on resulting reflectances as well as four derived indices (NDVI, PRI, CHL, and CAR) for the Laegern study site. Based on this analysis the merits and shortfalls of each approach are discussed and suggestions made for operational approaches which consider direct and diffuse irradiance fractions.

2 | Combining Imaging Spectroscopy, Digital Object Models, and 3D Canopy Modelling to Advance Retrievals of Vegetation Information over Forest Ecosystems

This chapter is based on:

Fawcett, D., Verhoef, W., Schläpfer, D., Schneider, F. D., Schaepman, M. E., & Damm, A. (in preparation). Combining imaging spectroscopy, digital object models, and 3D canopy modelling to advance retrievals of vegetation information over forest ecosystems. To be submitted to *Remote Sensing of Environment*

Contribution:	
Design	60%
Materials & Methods	75%
Results & Conclusions	90%

Abstract

Employing imaging spectroscopy techniques in vegetation analysis offers unique capabilities for assessing functional traits of plants. However, illumination effects challenge the retrieval of vegetation information from high spatial resolution airborne or satellite data in areas of complex topography. Accurate pixel-wise descriptions of direct and diffuse irradiance components are necessary to perform an atmospheric correction that yields representative surface reflectances. These irradiance components are determined by the atmosphere as well as illumination-observation-surface geometry. We evaluate three atmospheric correction strategies that differ in their complexity to simulate actual and pixel-wise fractions of diffuse and direct irradiances. All approaches are physically-based and use either bulk digital elevation models (DEM), fine resolution digital object models (DOM), or 3D modelling outputs from the Discrete Anisotropic Radiative Transfer (DART) model. By calculating accurate top-of-canopy reflectances for the Laegern test-site in Switzerland, we seek to improve retrievals of the Normalized Difference Vegetation Index (NDVI), the Photochemical Reflectance Index (PRI) as well as relative contents of chlorophyll and carotenoids. We demonstrate that both the DOM and the DART based approach improve the retrieval of above indices for flat cast-shadows by 15.3-71.1% compared to the simple DEM case. Over a dense forest area, improvements are less clear. Remaining issues are mainly overestimations of resulting surface reflectances and retrieved indices due to extreme illumination conditions. We expect these issues to be partly resolved if higher resolution auxiliary data and more precise irradiance simulations are used, which however largely increases processing time. Going forward we also emphasize the potential of vegetation information retrieval from at-sensor radiances as a more efficient and robust solution.

Keywords Imaging spectroscopy, Remote sensing, Atmospheric correction, APEX, Diffuse and direct irradiance, DOM, DART, NDVI, PRI, Chlorophyll, Carotenoids

2.1 Introduction

Vegetation ecosystems with their multitude of services are of great importance for human well-being: Provisioning of food, fuel, and fibre are the foundation of life and the fixation of carbon has become a much discussed topic in the face of climate change (Gifford, 1994; Schimel, 1995). The capability of vegetation to provide these services is influenced by a variety of environmental factors potentially limiting plant growth and the functioning of vegetation ecosystems (Nemani et al., 2003). Growing evidence indicates that environmental change increasingly impacts vegetation ecosystems and their supply of services, eventually affecting human well-being (Schröter et al., 2005). Lack of data and understanding, however, limits our capability to quantify and predict consequences of environmental change for humans and limits urgently required decisions to adapt to these changes. Remote sensing (RS) is suggested as a key technology to tackle the problem of data scarcity (e.g. Brunner et al., 2007; Kustas & Norman, 1996; Launay & Guerif, 2005). RS provides a unique capability to monitor spatio-temporal differences in vegetation functioning, health and status across scales by measuring important plant functional traits. Such information allows linking trends in vegetation changes with limiting factors and modelling future vegetation development by feeding the acquired information into expert systems, e.g., dynamic global vegetation models (DGVM) and land surface models (Cox et al., 2000; Rodell et al., 2004; Sitch et al., 2008). Increasing spectral resolution of optical sensors offers new opportunities in vegetation monitoring, which were not possible before. Besides biochemical plant traits (e.g., leaf chlorophyll and leaf water content), functional traits such as sun-induced chlorophyll fluorescence (SIF), non-photochemical quenching (NPQ), and light use efficiency (LUE) for use in estimating gross primary production (GPP) (Damm et al., 2015a; Porcar-Castell et al., 2014) can be retrieved nowadays. Such retrievals are achieved by exploiting narrow atmospheric absorption features to disentangle emitted SIF from reflected radiance signals or by measuring subtle changes of leaf absorption due to dynamics in the composition of xanthophyll pigments using the Photochemical Reflectance Index (PRI) (Gamon et al., 1992). Recent advancements in sensor technology allow combining high spectral with high spatial resolution. The information gained is, however, compromised by an increasing complexity in describing the radiative transfer of measurements. Highly resolved tree canopy measurements, for example, represent a mixture of sunlit and shaded crown parts, complicating retrievals of surface reflectance values as well as functional traits (Gastellu-Etchegorry et al., 1999). As RS strives to measure

ever smaller signals, for example SIF with ESAs upcoming Fluorescence Explorer (FLEX) Mission (Drusch et al., 2016), accounting for these kinds of effects has increasingly become a priority. A particular challenge is the estimation of surface irradiance, the main illumination source determining the radiative transfer of surfaces and vegetation canopies. Irradiance varies in its intensity as well as spectrally depending on its composition. Direct irradiance represents radiance on the direct path through the atmosphere while diffuse irradiance is scattered multiple times causing a wavelength dependent increase of the atmospheric pathway and thus an increase of atmospheric molecular absorption compared to the direct path. It has been demonstrated that these differences lead to considerable errors in retrieved surface reflectance and subsequently derived vegetation information if pixel-wise estimates of direct and diffuse irradiance are uncertain (Damm et al., 2015b). Accurate atmospheric correction of high spectral and spatial resolution imagery represents a challenge. The state of the atmosphere at acquisition time plays a vital role as variations in water vapour and aerosol load greatly impact spectral irradiance estimates (Cho et al., 2003). This necessitates a precise parameterization of the atmosphere for radiative transfer codes such as MODTRAN (Berk et al., 1989). Spatially, the complex irradiance fields required can no longer be described sufficiently by assuming uniformly flat Earth surfaces or by using coarse digital elevation models (DEM) as is common practice for the correction of satellite imagery (Richter, 1990, 1998). In literature, possible solutions to this problem have been discussed: A valid approach to minimize illumination effects is to only consider sunlit pixels in analysis (Malenovský et al., 2013). This, however, limits the exploitation of the full information available and, depending on the vegetation property derived, could lead to a bias. Yet other methods applied in post-processing frameworks after atmospheric correction include the use of matched filtering of reflectance data (Adler-Golden et al., 2002), but this lacks a true physical description of the issue. For more sophisticated approaches, the use of auxiliary data is suggested. A digital object model (DOM) of the scene derived from LiDAR data can be used to better represent the surface (Damm et al., 2015b). Ray tracing approaches on true 3D LiDAR data are also proposed (Schläpfer et al., 2003). In this study we hypothesize that (1) more accurate irradiance fields can be modeled by using auxiliary, scene specific data and that (2) these irradiance fields can be integrated within the atmospheric compensation process to generate reflectance and vegetation property products with minimized sensitivity to illumination effects. We evaluate three approaches for atmospheric correction that

are all based on the analytical four-stream theory (Verhoef & Bach, 2003) and account for direct and diffuse irradiance variations using different strategies. The first approach roughly estimates irradiance using a coarse DEM and serves as a reference for two more complex approaches. The second approach uses a DOM to determine irradiance by way of Hay's model for inclined surfaces (Hay & McKay, 1985). The third approach utilizes irradiance scaling factors derived from top-of-canopy (TOC) irradiances simulated by the 3D Discrete Anisotropic Radiative Transfer (DART) model (Gastellu-Etchegorry et al., 2015). All approaches are applied to an imaging spectroscopy (IS) flight line acquired with the Airborne Prism Experiment (APEX) sensor (Schaepman et al., 2015) to test the operational viability of these approaches. We further derive common vegetation indices sensitive for vegetation information including the Normalized Difference Vegetation Index (NDVI), the PRI and two pigment indices for chlorophyll (CHL) and carotenoids (CAR). Our results allow discussions on the viability of new processing strategies to compensate illumination effects in RS data and requirements when integrating auxiliary and RS data. We conclude with recommendations for future studies seeking to compensate irradiance effects in vegetation information estimated from RS data.

2.2 Data and study site

2.2.1 Study site

The Laegern study site is a limestone hill northwest of Zurich, Switzerland (47°28'54.75"N 8°23'37.82"E, 866m a.s.l.), stretching West to East. The site is mainly covered by a temperate mixed forest with a high diversity of tree species (dominated by beech, ash, sycamore and spruce) of different ages and sizes (Eugster et al., 2007). The Laegern is a well-studied site and contains a flux tower which is part of the AERONET (Holben et al., 1998) and FLUXNET (Baldocchi et al., 2001) measurement networks. The extent of the study site used here contains the Laegern forest as well as surrounding agricultural areas.

2.2.2 Imaging spectrometer data

The main datasets used are two flight lines covering the study site. They were acquired by APEX on the 26th of June 2010 at 15:30 UTC and on the 29th of June 2010 at 10:00 UTC. APEX is an airborne pushbroom imaging spectrometer covering the 372nm to 2500 nm region in 312 contiguous spectral bands. In this study, a spectral subset of the available bands is used, ranging from 399nm to 914nm, as these bands contain

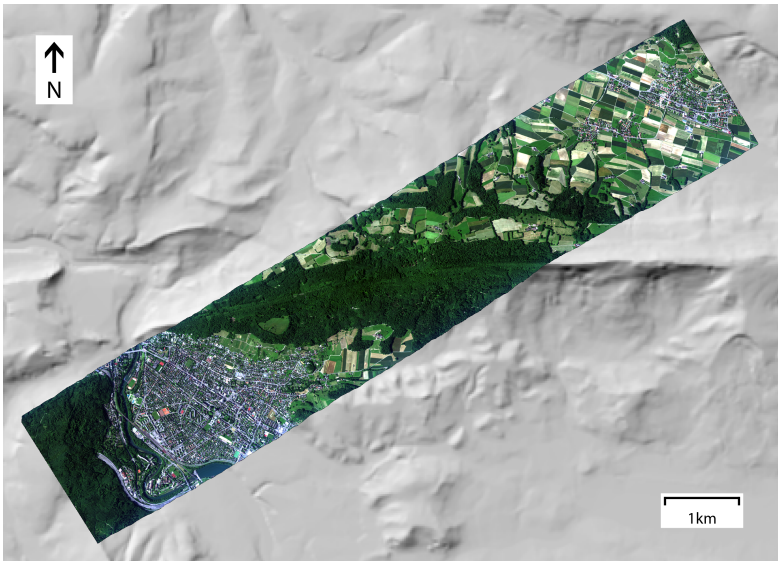

Figure 2.1.: APEX flight line (RGB composite of at-sensor radiance) of the Laegeren study site acquired on the 26th of June 2010. A hillshaded digital elevation model is used for the background (DHM25 (R) Swisstopo).

the necessary information to derive the desired vegetation indices and processing time is reduced. In this wavelength range, APEX shows a spectral sampling interval of 0.45-7.5 nm and a spectral sampling width of 0.86-15 nm (Schaepman et al., 2015). The data was pre-processed and provided as radiometrically, spectrally and geometrically calibrated radiances (level 1) (Hueni et al., 2009). The two datasets were then georectified using the PARGE software (Schläpfer & Richter, 2002). Most of the analysis is constrained to a spatial subset covering around 3.5 km^2 due to the smaller spatial extent of the auxiliary data (cf. sections 2.2.3 and 2.3.1.3). The dataset acquired on the 26th acts as primary dataset since it shows more extreme illumination conditions at acquisition time. The dataset of the 29th is used for cross-validation purposes.

2.2.3 Elevation models and derived datasets

Two elevation models are used in this study and act as the basis for further datasets. The first contains elevations derived from the Digital Height Model 25 (DHM25) data product (Swisstopo). The DHM25 resolves terrain elevation in 25 m spatial resolution and was interpolated to 2 m to match the pixel size of APEX. Where available, airborne laser scanning (ALS) based surface height measurements are smoothed with a large window low-pass filter and integrated in the DHM25. This preserves overall canopy height over

forested areas but single trees are not resolved due to the smoothing. This dataset is henceforth referred to as DEM (Digital Elevation Model). The second dataset features the unsmoothed ALS derived surface height information and is referred to as DOM (Digital Object Model). From the elevation models, datasets of slope, aspect and illumination were derived using the PARGE software, neglecting reflected terrain irradiance. The illumination value is represented by the cosine of the local illumination angle ($cos\theta_{il}$). For the DOM, a binary cast-shadow mask was calculated so that the illumination value equals zero in cast-shadows.

2.3 Methods

2.3.1 Atmospheric correction approaches

Atmospheric correction seeks to compensate atmospheric absorption and scattering effects on radiances measured by a sensor. Commonly used approaches can be separated into empirical and physical based approaches. Empirical approaches such as the Flat-Field approach (Roberts et al., 1986) are scene based and employ homogeneous surfaces to approximate and minimize atmospheric effects, eventually yielding relative reflectances. Physical or radiative transfer modelling approaches seek to simulate the absorption and scattering effects of atmospheric gases and aerosols using radiative transfer codes such as MODTRAN (Berk et al., 1989). Surface reflectances can finally be retrieved by combining observed radiance signals and modelled atmospheric quantities (Gao et al., 2009). According to Verhoef & Bach (2003), the radiative transfer in the atmosphere-surface system can be sufficiently approximated with the so-called four-stream theory comprising four spectral flux types. The fluxes considered are the downward solar flux, the diffuse downward flux, the diffuse upward flux and the upward spectral radiance in the direction of the observer. This study focuses exclusively on radiative transfer modelling approaches based on this theory to determine TOC hemispherical-conical reflectance factors (HCRF). To elaborate, irradiance is considered hemispherically while reflected radiances are measured by a sensor with a very small but non-zero IFOV (i.e., APEX IFOV is 0.025), which results in HCRF (cf. Schaepman-Strub et al. (2006) for details on terminology). Calibrated radiance data is processed to HCRF data using a simplified atmospheric correction approach compared to the state of the art atmospheric correction software ATCOR-4 (Richter & Schläpfer, 2002, 2016). The simplified approach includes the complete four-stream radiative transfer calculations but excludes atmospheric parameter retrieval, spectral polishing,

and radiometric fine tuning steps as implemented in ATCOR-4. We decided for a simplified atmospheric correction approach to ease evaluations and adjustments of atmospheric correction strategies. We also applied ATCOR-4 and used obtained HCRF as a reference to evaluate reliability of results stemming from the simplified atmospheric correction approach. In general, the atmospheric correction process can be divided into the following four steps: i) the simulation and storage of atmospheric transfer functions in look-up tables (LUT), ii) the estimation of spectral shifts and band broadening, iii) the convolution of the atmospheric functions considering the actual spectral sensor configuration, and iv) the calculation of HCRF values. The simulation of atmospheric functions is performed for five different ground heights using MODTRAN5 (Berk et al., 2006) and the MODTRAN interrogation technique as introduced by Verhoef & Bach (2003). Atmospheric variables water vapour and aerosol optical thickness (AOT), required to parameterize MODTRAN, were chosen based on sun-photometer measurements from a close by AERONET station (Holben et al., 1998) and ATCOR-4 image-based retrievals. The simulation of combined atmospheric functions (e.g., combined downward and upward transmittances) was performed in this step to avoid violation of the Beer-Lambert law in subsequent calculations with convolved functions (Verhoef et al., 2014). The estimation of potential spectral misregistrations, also known as spectral smile common to pushbroom spectrometers, and band broadening of APEX was performed with a method included in ATCOR-4 (Richter et al., 2011). Obtained spectral characteristics of APEX are used to generate spectral response functions to eventually convolve simulated atmospheric functions. The calculation of HCRF reflectances is based on the four-stream theory, using measured calibrated at-sensor radiances and simulated atmospheric transfer functions. This processing step provides the access point for testing different methods of reflectance calculation. Being computationally much less intensive than the other steps, it lends itself to experimentation while the previous steps resulting in the convolved LUTs are kept the same. The radiance data is then processed according to the steps described above while the method of simulating irradiance is varied in three steps of theoretically increasing accuracy (fig. 2.2). Each method requires a different set of auxiliary data as input. The three different methods are elaborated in the following sections.

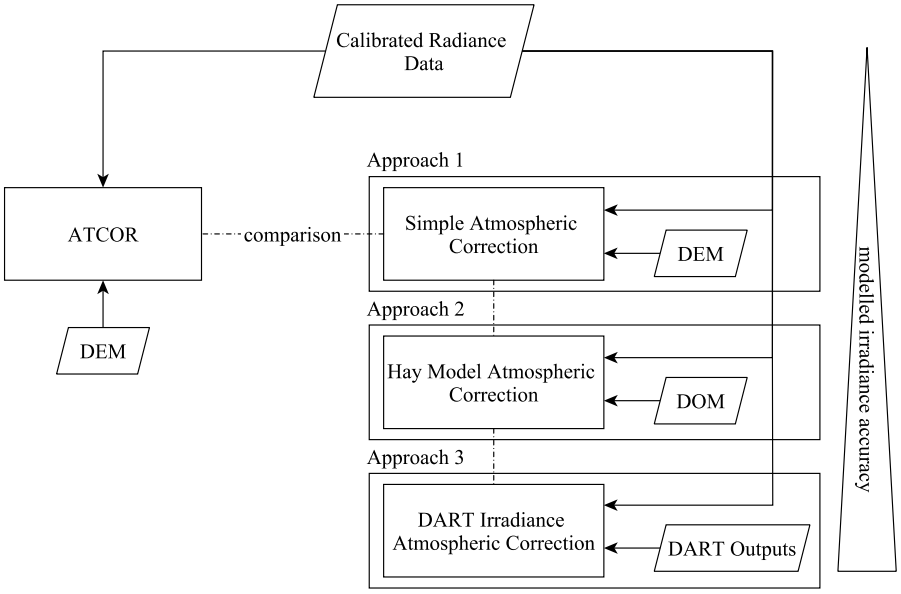

Figure 2.2.: Flowchart of data inputs and evaluated approaches.

2.3.1.1 Basic approach using a smoothed DEM

Verhoef et al. (2014) have used the four-stream theory to simulate top-of-atmosphere (TOA) radiances using combined models (e.g., SCOPE (Van der Tol et al., 2009), and MODTRAN4). According to them, the radiative transfer through the atmosphere yielding TOA radiance for a target (L_{TOA}) can be described as:

$$\begin{aligned} L_{TOA} =& \rho_{so}\frac{E_s^o \cos\theta_s}{\pi} \\ &+ \left[\frac{\tau_{ss} r_{so} E_s^o \cos\theta_s}{\pi} + SIF_s + \frac{(\tau_{sd} + \tau_{ss}\overline{r_{sd}}\rho_{dd})E_s^o \cos\theta_s/\pi + \overline{SIF_d}\rho_{dd}}{1 - \overline{r_{dd}}\rho_{dd}} r_{do}\right]\tau_{oo} \\ &+ \left[\frac{(\tau_{sd}\overline{r_{dd}} + \tau_{ss}\overline{r_{sd}})E_s^o \cos\theta_s/\pi + \overline{SIF_d}}{1 - \overline{r_{dd}}\rho_{dd}}\right]\tau_{do} \end{aligned} \tag{2.1}$$

Eq. (2.1) is formed by three additive terms including the atmospheric path radiance, the target's surface radiance, and the adjacency effect. The surface reflectance can be described by four terms: r_{so} is the bi-directional reflectance factor of the target (BRF), r_{do} the hemispheric-directional reflectance factor of the target (HDRF), $\overline{r_{sd}}$ is the smoothed directional-hemispherical reflectance factor of the surroundings (DHRF) and $\overline{r_{dd}}$ is the

smoothed bi-hemispherical reflectance factor (BHRF) of the surroundings. ρ_{so} is the atmospheric bi-directional reflectance and ρ_{dd} is the spherical albedo at the bottom of the atmosphere. τ_{ss} represents the direct atmospheric transmittance in sun-direction, τ_{oo} the direct atmospheric transmittance in view-direction, τ_{sd} the diffuse atmospheric transmittance for the solar incidence, and τ_{do} the directional atmospheric transmittance for diffuse incidence. E_s^o is the extra-terrestrial solar spectral irradiance on a plane perpendicular to the sun-rays. θ_s is the local solar zenith angle. SIF_s is the emitted SIF radiance of the target in observer-direction and SIF_d the hemispherical fluorescence flux of the surroundings (Cogliati et al., 2015). Eq. (2.1) can be written following the T-18 system as introduced by (Verhoef et al., 2014). When omitting the SIF contribution and adding viewing factors for direct and diffuse irradiance (V_{sun}, V_{sky}) (Verhoef & Bach, 2012), L_{TOA} of a non-Lambertian, non-uniform and tilted surface can be expressed as:

$$L_{TOA} \approx T_1 T_2 + \frac{T_1(T_8 r_{so} V_{sun} + T_9 r_{do} V_{sky} + T_{10}\overline{r_{sd}} + T_{11}\overline{r_{dd}})}{1 - \overline{r_{dd}} T_3} \tag{2.2}$$

While T_n represent atmospheric transfer functions (tab. 2.1), $\overline{r}$ indicate smoothed averaged reflectances and V_{sun}, V_{sky} can be expressed as:

$$V_{sun} = \cos\theta_t + \tan\theta_s \sin\theta_t \cos(\varphi_s - \varphi_t) \tag{2.3}$$

$$V_{sky} = \frac{1 + \cos\theta_t}{2} \tag{2.4}$$

V_{sun} and V_{sky} are scaling factors that express in a simple way how the direct irradiance of the sun and the diffuse irradiance of the sky are changed by the local topography. θ_t is the terrain slope inclination, φ_t the terrain slope azimuth, and φ_s the solar azimuth angle.

Table 2.1.: T-18 system of atmospheric functions. Angled brackets represent convolved quantities.

Atmospheric function	Name
$\langle E_s^o \rangle \cos\theta_s/\pi$	T_1
$\langle \rho_{so} \rangle$	T_2
$\langle \rho_{dd} \rangle$	T_3
$\langle \tau_{ss} \rangle$	T_4
$\langle \tau_{sd} \rangle$	T_5
$\langle \tau_{oo} \rangle$	T_6
$\langle \tau_{do} \rangle$	T_7
$\langle \tau_{ss}\tau_{oo} \rangle$	T_8
$\langle \tau_{sd}\tau_{oo} \rangle$	T_9
$\langle \tau_{ss}\tau_{do} \rangle$	T_{10}
$\langle \tau_{sd}\tau_{do} \rangle$	T_{11}

Assuming a Lambertian Earth surface, reflectance quantities can be assumed similar (i.e., $r_{so} = r_{do}$ and $\overline{r_{sd}} = \overline{r_{dd}}$) so that one can rewrite eq. (2.2) to yield TOC reflectance (r) from the measured at-sensor radiance (L_{TOA}). However, since $\overline{r}$ is still unknown, r must be estimated in two steps using a simplified version of eq. (2.2) where we assume a non-tilted, uniform Lambertian Earth surface and use low-pass filtered radiances ($\overline{L_{TOA}}$). A similar approach has been used in Richter (1998) but with smoothing the adjacency reflectance values.

$$\overline{r} = \frac{\overline{L_{TOA}} - T_1 T_2}{T_1(T_8 + T_9 + T_{10} + T_{11}) + (\overline{L_{TOA}} - T_1 T_2)T_3} \tag{2.5}$$

This finally allows a retrieval of r as follows:

$$r = \frac{(L_{TOA} - T_1 T_2)(1 - \overline{r}T_3) - \overline{r}T_1(T_{10} + T_{11})}{T_1(T_8 V_{sun} + T_9 V_{sky})} \tag{2.6}$$

This reflectance retrieval method is applied in combination with the smoothed DEM and further referred to as “DEM approach”.

2.3.1.2 Hay Model approach using DOM

The DEM approach assumes diffuse irradiance at target level as isotropic while in fact it is anisotropic with a large fraction centred on the direction of direct irradiance due to the forward scattering of aerosols. A more accurate way of modelling diffuse irradiance is required when working in complex canopies with extreme slopes and cast-shadows. Hay & McKay (1985) propose modelling diffuse irradiance on inclined surfaces (E^{dif}_{incl}) as a linear combination of an isotropic and a circumsolar component, dependent on the direct transmittance of the atmosphere τ_{ss}.

The isotropic component can be formulated as:

$$E^{dif}_{iso} = E^{dif}[(1-\tau_{ss})V_{sky}] \tag{2.7}$$

the circumsolar component can be formulated as:

$$E^{dif}_{cir} = E^{dif}[\frac{\tau_{ss}cos\theta_{il}}{cos\theta_s}] \tag{2.8}$$

while the combination of both can be expressed as:

$$E^{dif}_{incl} = E^{dif}K_{Hay} = E^{dif}[\frac{\tau_{ss}cos\theta_{il}}{cos\theta_s} + (1-\tau_{ss})V_{sky}] \tag{2.9}$$

E^{dif} is the total diffuse irradiance on the target assuming a flat surface, E^{dif}_{iso} denotes the isotropic component on an inclined surface and E^{dif}_{cir} the circumsolar component on an inclined surface. θ_{il} is the illumination zenith angle and $cos\theta_{il}$ is equivalent to $V_{sun}cos\theta_s$. K_{Hay} is the scaling factor to convert E^{dif} to E^{dif}_{incl}. By scaling diffuse radiance with K_{Hay} and not only with V_{sky} as in eq. (2.6), a better estimate for r of inclined surfaces can be retrieved with:

$$r = \frac{(L_{TOA} - T_1T_2)(1-\overline{r}T_3) - \overline{r}T_1(T_{10}+T_{11})}{T_1(T_8V_{sun} + T_9K_{Hay})} \tag{2.10}$$

The geometric surface description with a DOM yields V_{sun} values of 0 for strongly inclined tree canopies with slopes facing away from the sun as well as for cast-shadows. In fact, this can represent an underestimation of the direct irradiance in presence of small canopy gaps causing sun flecks and leads to extreme overestimates of HCRF. We applied a threshold value to keep direct irradiance from falling below 5% and, thus, to partly prevent these overestimates. This reflectance retrieval approach is referred to further as

the "DOM approach".

2.3.1.3 DART radiance output approach

The DART model (Gastellu-Etchegorry et al., 2015) is increasingly applied in vegetation analysis, for example as a tool to simulate at-sensor radiance data by parameterizing the model using LiDAR data (Schneider et al., 2014). The potential of such 3D radiative transfer modelling frameworks to derive accurate irradiance estimates has been suggested in previous work (Schläpfer et al., 2003). For our study site, LiDAR point cloud measurements were acquired by an ALS system close to the acquisition of APEX data. The point cloud was converted into a voxel grid and associated with different properties. A tree canopy voxel, for example, was assumed as turbid medium with certain leaf optical properties, plant area index (PAI) and a specific angular distribution of leaves (Gastellu-Etchegorry et al., 2015). For a detailed description of the parameterization of the 3D voxel grid, we refer to Schneider et al. (2014) and Schneider et al. (2015). DART is a coupled 3D canopy-atmosphere model, providing direct and diffuse irradiance components above the scene (BOA). An iterative ray-tracing technique is applied where direct irradiance is represented by parallel rays of photons in the sun direction and diffuse irradiance is tracked along discrete directions in 4π space (Yin et al., 2013). Within the scene, the first iteration represents the ray-paths until they are first intercepted. Intercepted energy by each voxel is stored. This produces the direct and diffuse sun illumination at TOC. Following iterations scatter and transmit the energy previously incident on each voxel until a defined number of iterations is reached, the energy of all rays falls below a certain threshold due to absorption or all rays leave the scene (Gastellu-Etchegorry et al., 2015). Due to computational constraints, only 24 directions were used and a maximum of 3 iterations were performed. Direct and diffuse irradiances at TOC were derived from DART simulation outputs as 2D grids of irradiance in W/m^2 for four wavelengths representing blue, green, red and NIR. Irradiance fractions per pixel (henceforth K_{dir} and K_{dif}) were derived relative to the maximum direct or diffuse irradiance, excluding outliers resulting from processing artefacts, and linearly interpolated for the wavelengths not simulated. The fractions can be applied directly as scaling factors for the direct and diffuse fluxes to retrieve r:

$$r = \frac{(L_{TOA} - T_1T_2)(1 - \overline{r}T_3) - \overline{r}T_1(T_{10} + T_{11})}{T_1(T_8K_{dir} + T_9K_{dif})} \tag{2.11}$$

This approach is referred to further as the "DART approach".

2.4 Deriving vegetation property products

A number of vegetation indices representing important functional plant traits were derived from TOC reflectance data to evaluate the impact of irradiance effects and their compensation using the three approaches under evaluation. Calculated indices include the NDVI, commonly used as a proxy for canopy chlorophyll content and fAPAR (Tucker, 1979) and the PRI, indicative for the de-epoxidation state of xanthophylls and often applied as proxy for LUE (Gamon et al., 1992, 1997). Further, we applied two indices sensitive to the relative content of chlorophyll and carotenoids as proposed by Gitelson et al. (2006).

$$NDVI = \frac{r_{800} - r_{640}}{r_{800} + r_{640}} \tag{2.12}$$

$$PRI = \frac{r_{531} - r_{570}}{r_{531} + r_{570}} \tag{2.13}$$

$$CHL \propto \frac{r_{790}}{\overline{r_{540-560}}} - 1 \tag{2.14}$$

$$CAR \propto \frac{r_{790}}{\overline{r_{510-520}}} - \frac{r_{790}}{\overline{r_{560-570}}} \tag{2.15}$$

Subscripts in eq. (2.14) and eq. (2.15) indicate wavelength ranges in nanometer used for the calculation of both indices. Gitelson et al. (2006) provide two models each for CHL and CAR, one incorporating green wavelengths and the other the red edge. We use the mean values over the proposed green wavelength ranges here as they should be more susceptible to differences in irradiance composition.

2.5 Results

2.5.1 Simple atmospheric correction in comparison with ATCOR

The implemented simple atmospheric correction approach allows efficiently and coherently evaluating possible strategies for the estimation of surface irradiance. An evaluation of the simple method with ATCOR-4 was applied to confirm its suitability for further

analysis. We particularly compared derived HCRF obtained from both approaches for two acquisition dates of a pseudo-invariant feature (fig. 2.3) and related them to surface HCRF measurements obtained with a field spectroradiometer (ASD FieldSpec, Analytical Spectral Devices, USA). For the 26th of June 2010, the mean difference in percent over all bands between the simple approach and ATCOR-4 is 35.4% and 16.4% for the 29th of June 2010. Considering ASD measured HCRF, the simple approach differs up to 4.2% for the 26th June and 25.3% for the 29th June. ATCOR-4 HCRF values differ from ASD measurements up to 24.9% for the 26th and 8.7% for the 29th. We observed a large difference of ATCOR-4 based HCRF for the two days of 42.2%, while this difference is only 20.9% for the simple approach. Absolute deviations of obtained HCRF values between the simple approach and ATCOR-4 are not detrimental for subsequent analysis. However, some differences appear to be wavelength dependent and require attention. Observed wavelength dependent deviations indicate persisting errors in the parameterization of the atmospheric status (i.e., aerosol load and distribution) and eventually in simulated LUTs, particularly for the 29th June. The compensation of adjacency effects was evaluated by observing the averaged HCRF of a black rooftop surrounded by vegetation (fig. 2.4). ASD measurements suggest a spectrally featureless reflectance behaviour with average values of 5%. There are no remnants of any vegetation signals visible in obtained HCRF spectra and barring a very slight slope towards NIR wavelengths, the adjacency effect compensation appears to be sufficient. It must be noted that HCRF values resulting from the simple correction were not smoothed or interpolated as is done in ATCOR; differences attributed to this were deemed negligible. ATCOR-4 also employs the Hay-model which was not included for this approach and could also cause slight differences.

Despite certain deviations between HCRFs obtained from ATCOR-4 and our simple implementation, the simplified atmospheric correction procedure was deemed to perform within sufficient accuracy to study the impact of irradiance effects and potential compensations using three strategies. Further, the dataset used for further analysis (26th of June 2010) shows HCRF values much closer to the reference HCRF compared to ATCOR-4 results.

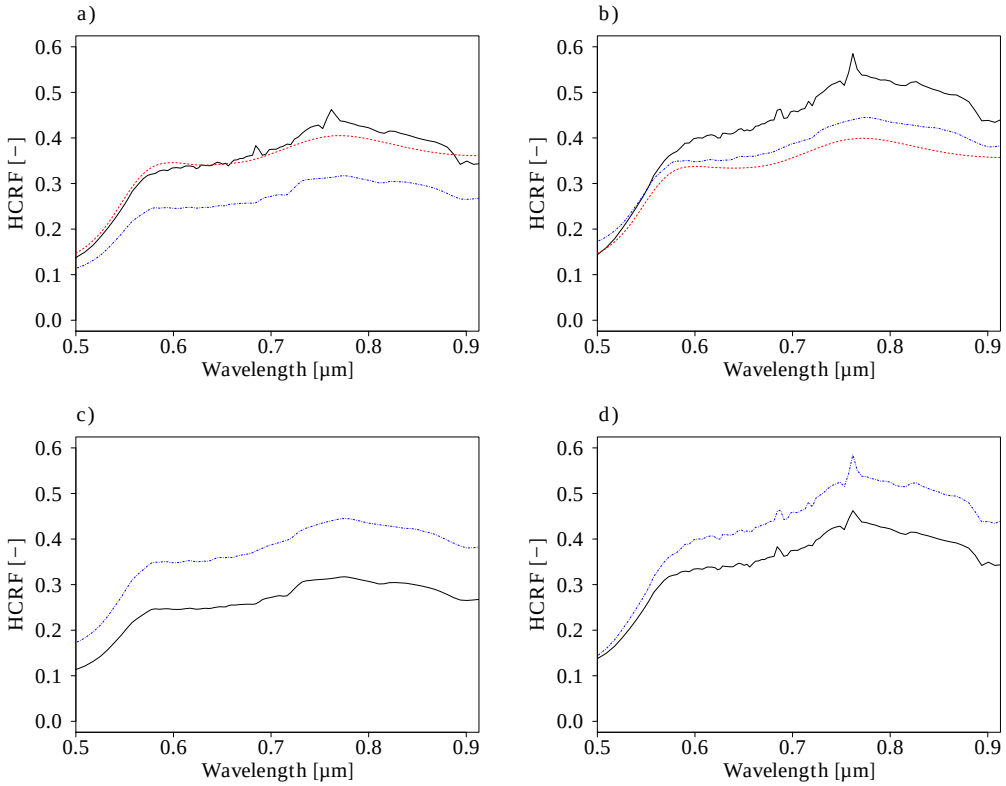

Figure 2.3.: Comparison of HCRF spectra for a yellow tartan sports-surface resulting from different atmospheric correction approaches. a) 26.06.2010 dataset. Solid black line: HCRF stemming from simple correction; dashed-dotted blue line: HCRF obtained from ATCOR-4; dashed red line: ASD measured HCRF. b) The same as in a but for the 29.06.2010. c) Solid black line: ATCOR-4 based HCRF for 26.06.2010; dashed-dotted blue line: ATCOR-4 based HCRF for 29.06.2010. d) Solid black line: HCRF from simple correction for 26.06.2010; dashed-dotted blue line: HCRF from simple correction for 29.06.2010.

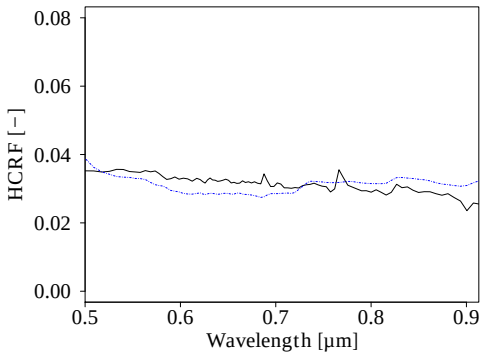

Figure 2.4.: Comparison of HCRF spectra averaged over a dark, spectrally uniform reflecting roof. Solid black line: HCRF obtained with the simple correction on 26.06.10; dashed-dotted blue line: ATCOR-4 based HCRF from the 26.06.10.

2.5.2 Improvement of atmospheric correction with DOM

The evaluated atmospheric correction incorporating a DOM to improve irradiance estimates considering crown geometry yields diverse results. Shaded canopy areas show overestimates of obtained HCRF values (above 100% reflectance) in case $\cos\theta_{il}$ drops below a certain threshold (e.g. 0.4 as visible in the canopy transect (fig. 2.5)). This is mainly since the slope angle (θ_t) for such canopy areas reduces the isotropic component of the diffuse radiation through V_{sky}. For sunlit canopy areas where $\cos\theta_{il}$ is larger than 0.4, HCRF differences are reduced. This observation can be confirmed by relating $\cos\theta_{il}$ and the per-pixel difference of HCRF at 800 nm obtained from the smoothed DEM and DOM approach for a large forest canopy subset (fig. 2.6): A coherent compensation of illumination effects appears for $\cos\theta_{il}$ values above 0.4 and the correction deteriorates for $\cos\theta_{il}$ below 0.3.

Areas affected by cast-shadows experience an improved correction of illumination effects when compared to fully illuminated regions (fig. 2.7). Exceptions are transition zones where the geometry-based cast-shadow mask does not perfectly overlap with those in the scene. The percentage deviation of retrieved HCRF in cast-shadows from illuminated canopy areas decreased on average over all bands from 85.7% for the smoothed DEM correction to 11.8% for the DOM approach. There are still deviations between calculated means of up to 41.1%, mainly around 500nm. We also note clearly visible remnants of absorption features at 760nm, 815nm and 900nm. Finally, it must be considered that the spatial difference between illuminated and shaded ROIs guarantee variance but this was

kept as small as possible.

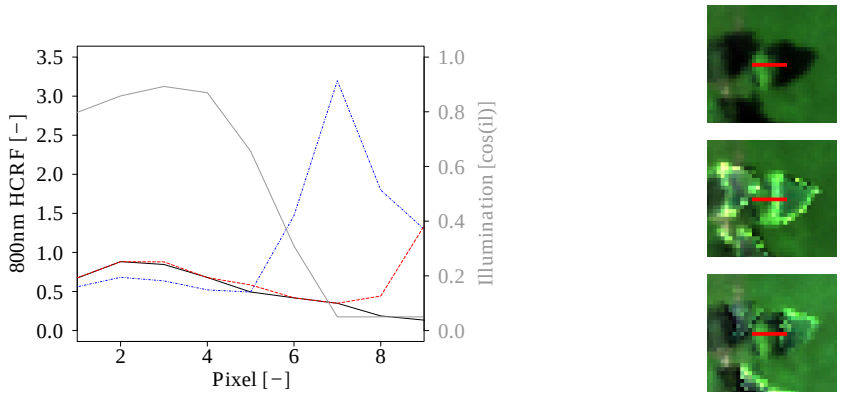

Figure 2.5.: Left: HCRF at 800nm along a tree-crown transect (left to right) for the smoothed DEM (black, solid), the DOM (blue, dashed-dotted) and the DART case (red, dashed). The grey solid line indicates changing illumination approximated by the illumination value $\cos\theta_{il}$. Right: Illustration of the transect for the DEM, DOM and DART based results (top to bottom).

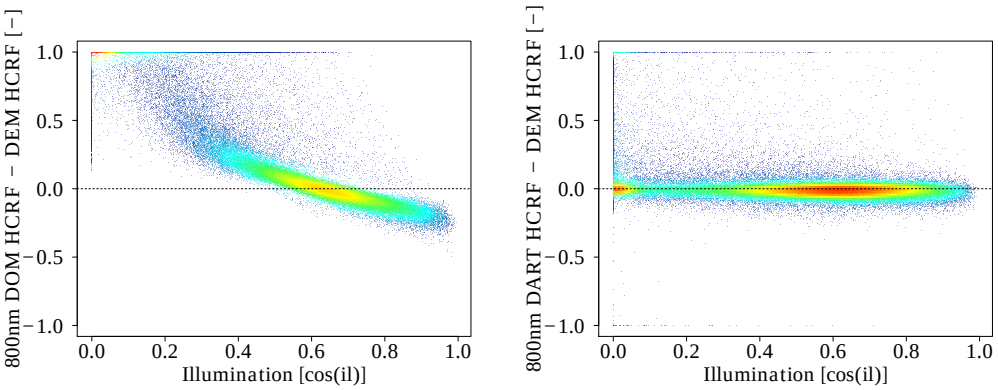

Figure 2.6.: Relation of illumination approximated with the value $\cos\theta_{il}$ and per pixel differences of HCRF at 800nm between the DOM approach to the smoothed DEM approach (left) and the DART approach to the smoothed DEM approach (right). Differences greater than 1 were set to 1 and those smaller than -1 were set to -1. The dashed line represents no change.

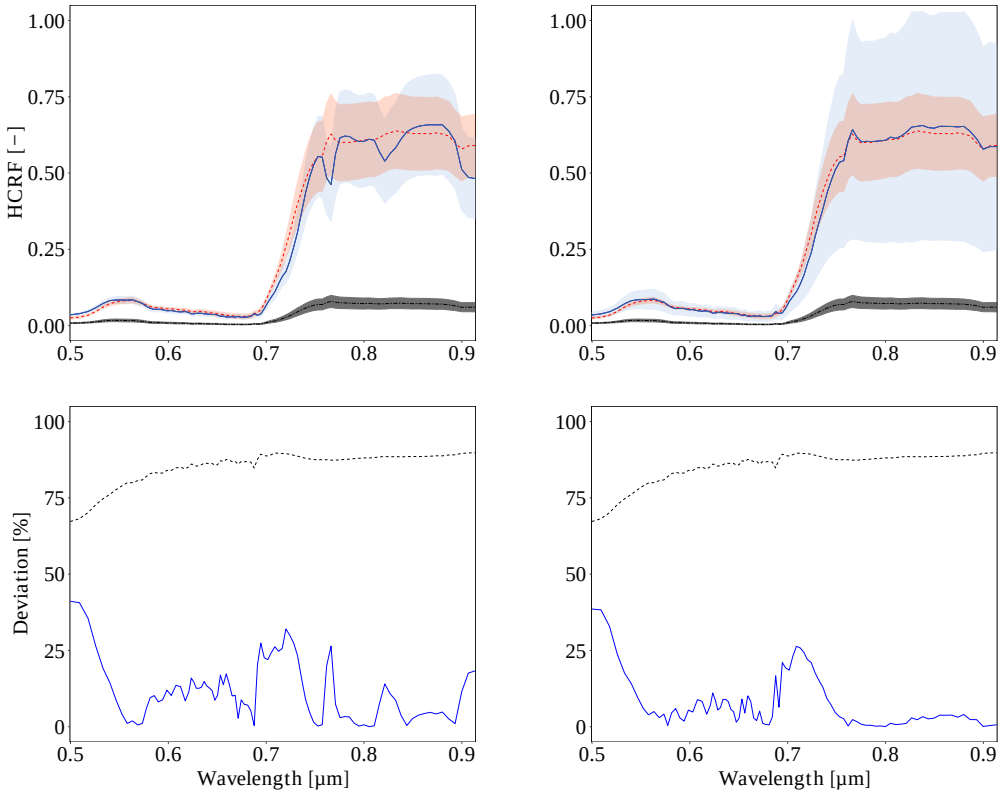

Figure 2.7.: Top: HCRF of shaded surfaces before and after correction. Left: Corrected HCRF averaged over cast-shadow regions of interest (ROI) on highly vegetated surfaces (blue solid line) as obtained from the DOM approach. The red dashed line indicates HCRF from the DEM approach averaged over fully illuminated ROIs on highly vegetated surfaces. Black dashed-dotted line: HCRF obtained from the smoothed DEM approach over cast-shadows in highly vegetated areas. Ribbons represent mean +- one standard deviation for each spectrum. Right: the same as left but for the DART approach. Bottom: Deviation in percent of the cast-shadow reflectances in respect to the fully illuminated case. Left: Deviation of the DEM approach HCRF (black dashed line) and the DOM approach (blue solid line). Right: the same as left but for the DART approach.

2.5.3 Improvement of atmospheric correction with simulated irradiance fractions

Using scaling factors derived from DART simulations to adjust estimates of diffuse and direct irradiance components in atmospheric correction approaches should in theory provide benefits over the DOM approach: They are ray-tracing based which allows accounting for multiple scattering within the canopy. Indeed, we observe fewer overestimates of HCRF values over tree canopies but reflectance gradients seem to have been

conserved for the most part (fig. 2.5). Overestimated HCRF values are mainly visible in transition zones from shade to full illumination, where we observe a spatial mismatch between simulated and actual cast-shadows in the order of up to two pixels (4m) in the most extreme cases, as well as for small gaps between trees in the forest. Evaluating corrected HCRF values at 800 nm over the forest subset, there appear to be generally lower reflectances compared to the DEM approach with a number of single pixels showing seemingly arbitrary high reflectance. These over estimated HCRF values are associated with the aforementioned gaps between trees where both direct and diffuse irradiance drop to near zero. We did not find a significant correction of shadowing effects across the tree canopies. This can be confirmed with an analysis of differences between HCRF obtained from the DART and the DEM approach and $\cos\theta_{il}$ (fig. 2.6). Since $\cos\theta_{il}$ was actually not used in the DART approach we would expect correlation to be slightly lower but still present if illumination effects were compensated. For flat cast-shadow areas, we found a far larger heterogeneity with small scale over and under corrections of HCRF values. When averaged, their reflectance is comparable to fully illuminated counterparts (fig. 2.7). Averaged over all bands, the deviation in percentage from illuminated areas to shaded counterparts has decreased to 7.8%. This represents a mean improvement over the smoothed DEM approach of 90.5%. The very large coefficient of variation of 47.5% has to be taken into account. The highest deviation between the averages is 38.6% and is observable in the red-edge. Towards the boundaries of the scene there is an increasing blue hue visible, especially in the corrected shadow regions. This effect is already slightly visible in the radiance data and therefore could be attributed to the fact that atmospheric parameters have been simulated for the nadir view case only.

2.5.4 Vegetation property products

The impact of illumination effects is clearly visible as brightness gradients in measured radiance images. In theory, after perfect atmospheric compensation, reflectance data would not be affected by these gradients unless they signify physiological changes. If the atmospheric compensation does not incorporate accurate pixel-based irradiances, reflectances are still dependent on illumination geometry which can lead to significant variations in derived physiological traits of the same area.

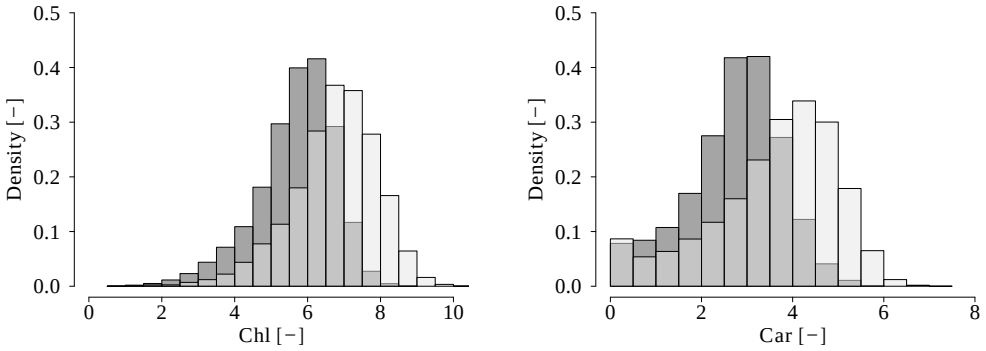

Figure 2.8.: Distribution of chlorophyll (left) and carotenoid (right) content index values for a forest subset. Bright grey: Values for 26.06.2010 at 15:30 UTC; Dark grey: Values for 29.06.2010 at 10:00 UTC. Index values were derived from ATCOR HCRF values.

For a forest subset of the APEX scene, we observe strong variations in retrieved CHL and CAR index values for contrasting illumination situations (fig. 2.8), illustrating the impact of illumination effects and the importance of accurate irradiance estimates to avoid them. The impact of varying direct and diffuse illumination on vegetation indices is larger in theory if spectral bands used are located at lower wavelengths (e.g. for CAR) where non-linear wavelength specific errors due to wrong irradiance estimates are the largest (c.f. Damm et al., 2015b). Corrections for illumination effects are therefore crucial for the estimation of diverse vegetation information including pigments. A successful correction not only increases the number of representative pixels in the scene, it would also facilitate the comparison of multi-temporal datasets and is necessary to track diurnal changes in photosynthetic efficiency by way of the xanthophyll cycle (Gamon et al., 1992) and SIF (Damm et al., 2010). The performance of the DEM, DOM and DART approaches presented here for the removal of illumination effects in vegetation products was evaluated by comparing obtained index values with reference values. We set up two experiments, the first evaluating the performance of the three approaches in cast-shadows, the second focussing on a forest subset. For the cast-shadow experiment, a number of areas were chosen and divided into sparsely and densely vegetated surfaces. The reference value is extracted over horizontal, fully illuminated areas of the same surface type in the DEM result. For the forest experiment, reference values represent the mean of horizontal oriented and fully illuminated areas (tops of tree canopies) extracted from the DEM result.

For both experiments, pixel-wise mean values of absolute differences between index and reference values were calculated. Pixel values outside of physically feasible ranges were omitted. Finally, the improvement of the DOM and DART approaches over the DEM approach was expressed as percentage by which the difference of the index to the reference value for the DEM approach could be reduced with either the DOM or DART approach. Differences between index and reference values larger than for the DEM case result in negative percentages while an equal difference corresponds to 0% and a full reduction of differences and therefore a perfect match of index with reference values corresponds to 100%. Results for all vegetation products are presented in tab. (2.2) and (2.3) for the cast-shadow experiment and for the forest experiment in tab. (2.4). A paired t-test with 95% significance level ($p << 0.05$) indicates that mean values of all DOM and DART results are significantly different from the DEM result. Fig. (2.9) illustrates results for a subset of the scene containing a heterogeneous vegetation cover and illumination conditions.

NDVI

The difference in NDVI between shaded and fully illuminated areas is small for dense vegetation and larger for sparse vegetation cover. Applying both, the DOM and the DART approach yields slightly overestimated NDVI values in cast-shadow for densely vegetated surfaces. The reduction of illumination effects is small, roughly 15%. For sparse vegetation the improvement is over 50%, with slight underestimations in DOM results and overestimations in DART results. For the forest subset, the DOM approach introduces overestimations of NDVI values and increases the difference while the DART approach yields results close to the DEM result.

PRI

For the PRI, differences between shaded and fully illuminated areas are large for dense and sparse vegetation cover. Applying both, the DOM and the DART approach yields slightly overestimated PRI values in cast-shadow. The reduction of illumination effects is large: for sparse vegetation the improvement is between 39% for the DOM approach and up to 71% for the DART approach. A similar picture can be observed for dense vegetation. For the forest subset, the DOM approach introduces slight overestimations of PRI values but slightly reduces uncertainties while the DART approach yields results close to the DEM result.

Chlorophyll

Both, the DOM and the DART approach yield consistent improvements of CHL estimates compared to the DEM approach of over 50% for cast-shadows in sparse and dense vegetation. The DART approach performs better with 63.1% for sparse vegetation but also more than doubles the standard deviation. The DOM approach shows higher consistency across surface types. The improvements for cast-shadows are clearly visible in Fig. (2.9), however, trees clearly display an overestimation of retrieved chlorophyll content in the DOM-based result (52.4%). For the DART approach, chlorophyll is slightly underestimated.

Carotenoids

Retrieved carotenoid contents in cast-shadow show the same pattern of improvement as for the chlorophyll content. The DOM approach yields an improvement of around 37% while the DART approach performs better, reducing the difference between CAR estimates in illuminated and shaded canopy parts by 41% for densely vegetated areas and 55.6% for sparsely vegetated areas. Mean values are much closer to the reference but the standard deviation is clearly increased, accounting for the medium reduction overall. For the forest subset there is no improvement regarding the pixel-wise differences from the reference value.

Table 2.2.: Impact of illumination effects on NDVI, PRI, chlorophyll and carotenoid retrievals for densely vegetated surfaces. Index values in cast-shadow and fully illuminated areas were compared. The compensation of illumination effects using three atmospheric correction strategies (DEM, DOM and DART approaches) was evaluated. Calculated statistics include mean, standard deviation, mean pixel-wise absolute difference to the illuminated reference value and percent reduction of this difference in respect to the DEM case.

NDVI				
	Mean	StDev	Abs Diff	% Diff reduced
Reference	0.862	0.043	-	-
DEM	0.848	0.037	0.032	-
DOM	0.880	0.029	0.027	15.3
DART	0.870	0.032	0.026	16.9
PRI				
	Mean	StDev	Abs Diff	% Diff reduced
Reference	-0.011	0.014	-	-
DEM	0.101	0.018	0.112	-
DOM	0.063	0.018	0.074	34.1
DART	0.040	0.025	0.053	53.1
CHL				
	Mean	StDev	Abs Diff	% Diff reduced
Reference	6.450	1.264	-	-
DEM	3.422	1.064	3.065	-
DOM	6.198	1.608	1.314	57.1
DART	5.863	1.693	1.466	52.2
CAR				
	Mean	StDev	Abs Diff	% Diff reduced
Reference	7.461	2.396	-	-
DEM	1.583	0.634	5.877	-
DOM	3.771	1.252	3.703	37.0
DART	4.085	1.656	3.466	41.0

Table 2.3.: Impact of illumination effects on NDVI, PRI, chlorophyll and carotenoid retrievals for sparsely vegetated surfaces. Index values in cast-shadow and fully illuminated areas were compared. The compensation of illumination effects using three atmospheric correction strategies (DEM, DOM and DART approaches) was evaluated. Calculated statistics include mean, standard deviation, mean pixel-wise absolute difference to the illuminated reference value and percent reduction of this difference in respect to the DEM case.

NDVI				
	Mean	StDev	Abs Diff	% Diff reduced
Reference	0.478	0.032	-	-
DEM	0.361	0.074	0.123	-
DOM	0.469	0.066	0.051	58.7
DART	0.496	0.075	0.059	52.4
PRI				
	Mean	StDev	Abs Diff	% Diff reduced
Reference	-0.063	0.009	-	-
DEM	0.030	0.021	0.093	-
DOM	-0.007	0.020	0.057	39.0
DART	-0.041	0.022	0.027	71.1
CHL				
	Mean	StDev	Abs Diff	% Diff reduced
Reference	2.143	0.225	-	-
DEM	0.584	0.316	1.559	-
DOM	1.560	0.488	0.665	57.3
DART	1.858	0.669	0.576	63.1
CAR				
	Mean	StDev	Abs Diff	% Diff reduced
Reference	1.014	0.193	-	-
DEM	0.072	0.096	0.942	-
DOM	0.433	0.185	0.589	37.5
DART	0.849	0.463	0.418	55.6

Table 2.4.: Impact of illumination effects on NDVI, PRI, chlorophyll and carotenoid retrievals for a forest canopy. Index values in shadow and fully illuminated areas were compared. The compensation of illumination effects using three atmospheric correction strategies (DEM, DOM and DART approaches) was evaluated. Calculate statistics include mean, standard deviation, mean pixel-wise absolute difference to the illuminated reference value and percent reduction of this difference in respect to the DEM case.

NDVI				
	Mean	StDev	Abs Diff	% Diff reduced
Reference	0.910	0.020	-	-
DEM	0.911	0.026	0.016	-
DOM	0.916	0.025	0.018	-8.5
DART	0.910	0.026	0.017	-1.6
PRI				
	Mean	StDev	Abs Diff	% Diff reduced
Reference	-0.014	0.016	-	-
DEM	-0.002	0.036	0.023	-
DOM	-0.010	0.031	0.020	12.4
DART	0.000	0.032	0.023	2.6
CHL				
	Mean	StDev	Abs Diff	% Diff reduced
Reference	9.523	1.808	-	-
DEM	9.549	1.928	1.471	-
DOM	10.789	2.852	2.242	-52.4
DART	9.294	2.014	1.527	-3.7
CAR				
	Mean	StDev	Abs Diff	% Diff reduced
Reference	10.314	1.908	-	-
DEM	9.252	2.753	2.211	-
DOM	10.691	3.010	2.266	-2.5
DART	8.927	2.593	2.235	-1.1

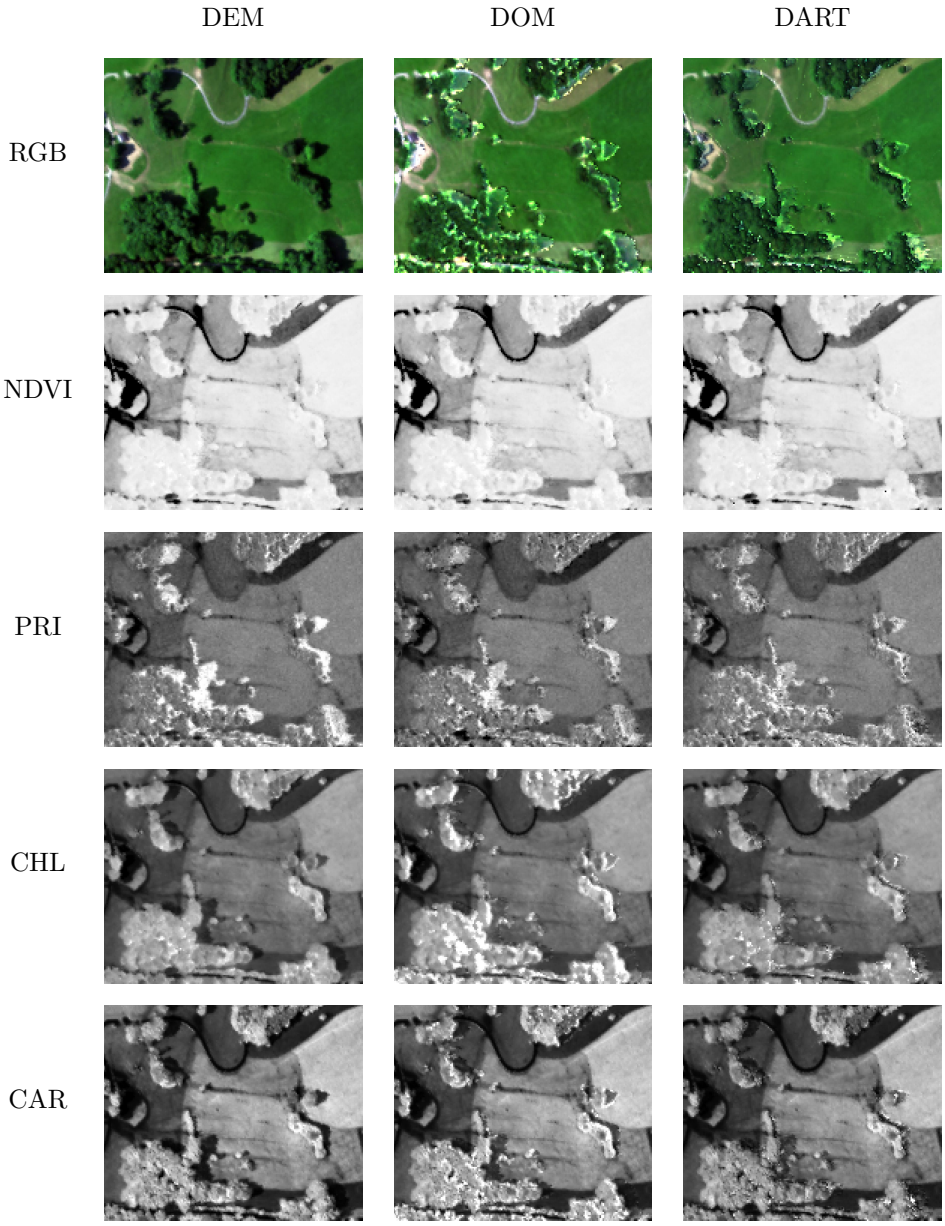

Figure 2.9.: Impact of illumination effects on HCRF data and subsequently calculated vegetation indices. Results indicate the impact and compensation considering three different atmospheric correction approaches. Displayed are the RGB representation and vegetation products (NDVI, PRI, chlorophyll and carotenoids) for a subset of the scene including fields, trees and cast-shadows.

2.6 Discussion

2.6.1 Reliability of the implemented simplified atmospheric correction approach

We evaluated the performance of three atmospheric correction approaches that differ in their strategy and complexity to approximate direct and diffuse irradiance fields. Since off the shelf atmospheric correction approaches are difficult to modify, a simple atmospheric correction scheme based on the four-stream theory was implemented (Verhoef & Bach, 2003). A comparison of the simplified atmospheric correction with ATCOR-4 indicates a good agreement but also reveals several differences and general issues inherent to atmospheric correction approaches. Retrieved surface reflectance of a pseudo-invariant surface largely varied between two acquisition times ($\sim$ 20% for our approach). This effect is even larger for ATCOR-4 results ($\sim$ 42%), indicating inherent uncertainties in atmospheric correction even if sophisticated correction procedures are applied. It is possible that this variation can be partly explained by the difference in solar zenith angle (48.1° vs. 29.3°) in combination with reflectance anisotropy effects. However, for the homogeneous reference surface investigated, such a strong influence is unlikely. We expect erroneous estimates of surface irradiance as main cause for this finding. Although our simplified implementation shows a smaller difference in HCRF across the two acquisition dates, they appear wavelength dependent. Wavelength dependent differences are also found in the direct comparison with ATCOR-4 results. This finding indicates an imperfect parameterization of the atmosphere (e.g., AOT). There are three main differences in the atmospheric correction: i) ATCOR-4 uses the horizon algorithm providing a more accurate value for V_{sky} than the slope based calculation used in our simplified approach, relevant considering the topography in the scene. ii) In the chosen ATCOR-4 configuration, atmospheric conditions are specified with a constant AOT across the scene but varying water vapour over the image. iii) ATCOR-4 uses viewing angle dependent scattering functions for the correction of aerosol effects. In the simplified version, atmospheric parameters were obtained from AERONET and ATCOR-4 and only distributed considering ground and sensor height. A comparison of HCRF of a uniform dark reference target indicates that adjacency effects are adequately corrected on par with ATCOR-4 results, demonstrating the suitability of both approaches to accurately represent values of shaded regions.

2.6.2 Reliability of approaches to advance estimates of direct and diffuse irradiance

2.6.2.1 Irradiance estimates using smoothed elevation models

Many simple atmospheric correction methods assume flat Earth surfaces and need minimal inputs to calculate reflectance (e.g. Ouaidrari & Vermote, 1999; Richter, 1990). These approaches are not suitable for high resolution imagery and/or complex terrain. In early approaches seeking to compensate terrain influences, the cosine correction based on $\cos\theta_{il}$ is applied (often directly to TOA radiances), using a DEM (Teillet et al., 1982). However, it was observed to be unsuitable for terrain containing steep inclines where the solar incident angle approaches 90° or above (Itten & Meyer, 1993; Teillet et al., 1982). Results of our simple approach show no extreme overestimations of HCRF due to the use of a smoothed DEM. This strategy eliminates abrupt changes in geometry and diffuse irradiance estimates in relation to $\cos\theta_t$. However, since the DEM does not include single canopy geometries, correct irradiance fractions for tree crowns and cast-shadows cannot be estimated. Small-scale illumination based reflectance variations persist.

2.6.2.2 Advanced estimates of direct and diffuse irradiance using DOM

The use of a DOM yields more uniform surface reflectances across illumination angles, allowing a better comparison of canopy parts described as at the top of canopies with canopy parts oriented towards and slightly oriented away from the sun ($\cos\theta_{il} = 1 :\sim 0.4$). Further, the DOM based atmospheric correction strategy yields a significantly improved HCRF estimate for flat cast-shadows (86% on average over the DEM approach). However, we also observed too high HCRF values for canopy areas where $\cos\theta_{il}$ is small and the surface slope is steep. Such high HCRF values in shaded parts of tree canopies are due to an underestimation of irradiance, rendering an inherent problem in the DOM's 2.5-dimensional smooth description of canopy surfaces (Schläpfer et al., 2003). In regions with steep slopes, direct irradiance and circumsolar diffuse irradiance tend toward zero while isotropic diffuse irradiance is also reduced due to the slope. While the used Hay's model has been successfully applied to correct for illumination effects in rugged terrain using a DEM (Sandmeier & Itten, 1997), single tree canopies represent a more complex problem challenging the application of Hay's model. Studies using Hay's model and a DEM also report overestimates of HCRF and put these down to inadequate spatial resolution of the DEM (Sandmeier & Itten, 1997). In our case, this could be partly counteracted by a DOM

resolution which is considerably higher than the image pixel size. We expect that the main cause for observed reflectance overestimates is neglecting the fact that the canopy structure is 3-dimensional, with factors such as leaf orientation influencing actual irradiance. The binary nature of the applied cast-shadow mask causes an under estimation of both the direct and circumsolar diffuse irradiance. Further, cast-shadows on flat surfaces receive an overestimated amount of isotropic irradiance due to the slope-based calculation. It is likely that these effects cause the observed deviations in the absorption bands between the corrected and illuminated reference regions. Commonly used elevation-model based atmospheric correction approaches solve the problem of HCRF overestimations by applying non-Lambertian methods with empirical and image-derived correction factors (Riaño et al., 2003). ATCOR-4 contains a combined atmospheric and topographic correction called integrated radiometric correction (IRC) (Kobayashi & Sanga-Ngoie, 2008), a semi-empirical method that includes a regression analysis of $L_{TOA} - T_1 T_2$ versus $\cos\theta_{il}$ (using our notation) over the entire image to calculate radiances from inclined surfaces. A comparison of approaches yielded the best results for the Modified Minnaert method which includes correction factors varying with illumination angle thresholds and land-cover type (Richter et al., 2009; Richter, 1998). These approaches are however mostly designed to correct large scale topography effects in mountainous regions in coarse spatial resolution satellite images. The application of such corrections to 2.5-dimensional surface models of heterogeneous vegetation canopies (e.g., forest) at all, even if available in a resolution adequate for airborne scanner data, has been called into question due to their neglect of multiple scattering effects within crowns (Schläpfer et al., 2003). Seeing that our results were promising for certain irradiance conditions, we should not rule out that an approach using optimized correction factors for canopy areas with extreme illumination conditions could further advance retrieved products. They must be empirically derived but possibly based on outputs of canopy radiative transfer simulations. As an alternative to deriving surface irradiance from a DOM that is highly dependent on the DOM's resolution and co-registration accuracy, empirical cast-shadow detection approaches could be applied to quantify shading and, thus, to constrain estimates of diffuse and direct irradiance. A proposed method uses a red-blue index combined with empirical factors to discern the diffuse irradiance fraction per pixel. Further, indices have to be used to make the method applicable to any surface type (cf. Schläpfer et al. (2013) for a full description). There are a number of drawbacks to this method, chiefly the changing of absolute reflectance values

and, thus, the range of subsequently derived vegetation indices and plant trait products.

2.6.2.3 Advanced estimates of direct and diffuse irradiance using the DART model

We observed that HCRF values resulting from an atmospheric correction that incorporates a scaling of direct and diffuse irradiance based on DART irradiance outputs show no comprehensive improvements in tree canopies compared to the simpler DEM approach. HCRF gradients due to varying illumination over the canopies are mostly preserved while gaps in and between canopies exhibit overestimates of retrieved HCRF. For cast-shadows, however, the DART approach yields better results: Averaged HCRF values within a cast-shadow closely resemble those for fully illuminated areas of the same vegetation cover. There is however a high spatial variation of retrieved HCRF within these cast-shadow areas. A primary source of uncertainty when driving the final HCRF products are the irradiance scaling factors as obtained from DART: DART simulations were limited in their complexity due to computation time constraints. The spatial distribution of resulting diffuse scaling factors display a considerable deviation from the expected spatial distribution as obtained for direct irradiance. This kind of spatial mismatch is caused by an insufficient number of possible scattering directions during the simulation (personal communication with D. Kükenbrink, UZH). A full convergence of diffuse and direct cast-shadows requires several hundreds to thousands of scattering directions in 4π space (as opposed to the 24 used in this study), requiring considerable processing power and time. Studies using DART to simulate RS data of smaller scenes use 100+ angles (Gastellu-Etchegorry et al., 1996; Schneider et al., 2014). An efficient method to improve the simulation of canopy multiple scattering is an oversampling of certain angular regions, for example of the hot-spot configuration (Yin et al., 2013). 100 scattering angles over the sphere and a further 100 for the hot-spot has been shown to also result in a sufficient overlap of the cast-shadows and is therefore highly recommended for further studies of irradiance effects with DART like models (personal communication with D. Kükenbrink, UZH). Concerning scattering iterations, it is likely that multiple scattering effects as present in canopy gaps require more than three iterations to be adequately described: A sensitivity analysis on smaller scene subsets is recommended to find the appropriate parameterization of DART. The lack of variation in simulated direct irradiance over the canopy is a primary reason for the persistence of illumination gradients in HCRF outputs. This can be attributed to the voxel size being too large to accurately approximate the canopy shape, especially as there is no slope information to scale irradiance in this approach. The voxel size of 2x2x2

m corresponds to the image pixel size of 2x2 m but ideally the resolution used for the radiative transfer simulation would be higher and up-scaled to sensor resolution (Malenovský et al., 2007). The use of DART irradiance simulations is an interesting strategy to facilitate a physical based approach for atmospheric correction. Based on our findings, there are however a fair number of requirements that must be met in order to perform an adequate reflectance retrieval. The most limiting factor is the availability of LiDAR data that show a high co-registration accuracy with IS data. Additionally, there is a temporal constraint in that a larger time lag between the acquisition of forest structure through LiDAR and the optical data can cause deviations due to tree growth and logging. In this study, we benefitted from data acquired in the same year. Further, there must be a large computational capacity available to perform a DART simulation with a sufficient number of scattering angles and iterations as well as voxels ideally an order of magnitude smaller than the image resolution. These preconditions were only partially met by this study and further research should be performed to quantify their importance. Finally, an accurate parameterization of the atmosphere is crucial as AOT strongly influences diffuse irradiance. It should be noted that the strength of the DART model lies in its capability of simulating radiative transfer through complex vegetation canopies and ultimately at-sensor radiances. While we demonstrated that there is added value in using DART derived scaling factors, these are only based on simulated TOC irradiances.

2.6.3 Improvement of plant trait product retrieval using advanced atmospheric correction

In general, derived plant trait products based on vegetation indices are less sensitive to uncertainties induced by atmospheric correction approaches compared to reflectance retrievals. However, substantial uncertainties in vegetation products caused by inappropriate estimates of surface irradiance in atmospheric correction approaches urgently require the development of advanced retrieval strategies. Both evaluated approaches lead to significantly improved retrievals of vegetation indices, and thus, plant trait products in cast-shadow. The DOM approach provides advanced estimates of all vegetation indices analysed. Also the DART approach shows overall improved estimates of vegetation indices, while mean values in cast-shadows are very close to those of illuminated surfaces. Improvements are comparable for all vegetation indices and surfaces ($\sim 50\%$ on average). The drawback of the DART approach is a wide spread of values that can be attributed

to the limitations imposed on the simulation as discussed above. Results are more diverse across illumination conditions as apparent in forest canopies. While no effect was found for the CAR index, the evaluated DOM approach shows spatially more consistent vegetation index values across canopies for PRI but slightly worse results for NDVI and substantially worse for CHL. The calculation of PRI incorporates wavelength regions in the visible strongly affected by fractional changes of direct and diffuse irradiance; applied corrections using Hay's model seem to improve HCRF retrievals at such wavelengths. Instead, the calculation of NDVI and CHL incorporates reflectances values in the NIR that are exaggerated if modelled direct irradiance is too small. Wavelength dependent improvements of the applied DOM approach mainly affect the visible and less the NIR. This might explain the increasing sensitivity of both indices for illumination effects when using the DOM approach. Results based on highly overestimated HCRF values should be taken with caution in all cases and possible effects evaluated. Previous studies have also identified the issues of using TOC irradiances to derive vegetation indices as they fail to account for within-canopy irradiance effects and resolve the issue by applying correction factors to the index (Takala & Mõttus, 2016). Over dense forest canopies, there seems to be no advantage in using irradiance estimates obtained from DART simulations; results are overall very similar to the DEM case or slightly worse. The lacking variability in modelled direct irradiance is the primary cause for this. It is likely that the smoothed DEM still provides a better approximation of canopy surfaces than the surface described by the voxel grid. A final issue of note is that we evaluated the improvement of plant trait retrievals by comparing estimates of partly shaded canopy areas to those of illuminated canopy areas. This strategy assumes that reflectances and thus plant traits are identical across illumination conditions if fully corrected. This is an imprecise assumption as the difference is not entirely due to wrong irradiance estimates but also surface properties and plant physiological responses. According to the four-stream theory, reflectance factors for diffuse and direct irradiance are different, causing a variation in retrieved surface reflectance and vegetation indices as function of illumination conditions. Further, the PRI has been shown to vary throughout the day based on illumination, being enhanced in low-light conditions (Gamon & Bond, 2013). Yet other studies imply a strong link between the xanthophyll cycle pigment changes and PRI of varying canopy shadow fractions (Hall et al., 2008). The effect of diffuse irradiance on directional PRI is deemed to be of the same magnitude as the physiological response (Mõttus et al., 2015). Separating the

three influences on measured plant trait products represents a challenge and would require extensive field physiological sampling. This issue is especially limiting when seeking to derive SIF values free of any illumination effect, as SIF shows a strong physiological response with irradiance (Damm et al., 2015b).

2.6.4 Towards advanced physically-based vegetation product retrievals

The primary drawback of all approaches presented here was found to be the inaccuracy in estimating surface irradiances including its direct and diffuse components. This limitation is mainly caused by inadequate auxiliary data and over simplifications of the radiative transfer within canopies. The latter will cause errors in TOC reflectances regardless of the DOM resolution or the DART irradiance simulation capability. The most accurate retrieval of plant trait products requires to forgo TOC reflectances altogether by applying a method that describes the radiative transfer in the coupled atmospheric canopy system and moving the retrieval problem to the at-sensor radiance level. Such TOA approaches are the focus of latest studies seeking to derive vegetation information from satellite (simulated) and airborne imagery (Laurent et al., 2014). The TOA approach allows a direct comparison of simulations with measurements since they are of the same physical quantity (Verhoef & Bach, 2003). Apart from strictly following the sequence of physical interactions and minimizing assumptions, other benefits of simulating TOA radiances are the inclusion of topography, adjacency and surface anisotropy effects in the forward model and during the ultimate retrieval of plant trait products (Laurent et al., 2011). This is in strong contrast to TOC approaches where errors propagate due to i) the sequential processing (e.g., posterior anisotropy correction), ii) the retrieval of plant traits via indices and empirical models, and iii) the comparison of different physical quantities (i.e., BRF from canopy radiative transfer models versus HCRF derived from measurements (Laurent et al., 2011)). In theory, the model inversion can also yield the distribution of direct and diffuse illumination which represents a major advantage, but at the cost of increasing the ill-posedness of the problem (Combal et al., 2003). In an implementation of this approach by Laurent et al. (2011), the at-sensor radiances are simulated by coupling the atmospheric radiative transfer model MODTRAN4 and the surface model SLC (Verhoef & Bach, 2007) describing soil-leaf-canopy interactions. The estimation of vegetation variables is improved using a Bayesian object-based approach with a priori information to enable a more efficient inversion by avoiding unlikely variable combinations. Novel approaches using Monte Carlo Markov Chains (e.g. Gilks et al., 1996) instead of

Bayesian methods are currently being developed. These allow a sampling of the desired parameter's space based on its probability distribution function. By using MCMC methods it is also hoped that the retrieval of multiple parameters is simplified, making it the most promising approach to derive accurate irradiance fractions. Areas where further development is needed for the operational implementation of the TOA methods are adjacency and topography effects as well as the large computation time (Mousivand et al., 2015).

2.7 Conclusions

We provide further evidence that scene reflectance and derived vegetation products are considerably uncertain if the relative contribution of direct and diffuse irradiance to total irradiance is not estimated accurately. We conclude that improvements in the retrieval of surface reflectance and plant trait products by ingesting further auxiliary data to account for varying irradiance fractions in atmospheric compensation approaches are limited. Using a DOM or DART simulated irradiance fractions to estimate irradiance leads to some improvements over a simplified approach using spatially coarse resolution DEMs. However, a number of issues and requirements were identified limiting the applicability of the two proposed approaches. This includes the resolution of the DOM and DART voxel grid that should ideally be an order of magnitude larger than the image data. Further, applied approaches are limited in their physical representation of the complex radiative transfer in heterogeneous canopies. The DOM approach being 2.5 dimensional represents an oversimplification while the DART based approach requires a very large number of scattering angles and iterations to accurately simulate irradiance. We propose further investigating other options which are promising as operational solutions. Going forward, we emphasize the potential of TOA approaches to derive accurate irradiance fields and vegetation variables.

3 | Synthesis

High spatial resolution spectral information is in demand because it enables novel analysis techniques and the application of RS in new scientific fields. A prime example is RS of biodiversity through direct approaches like classifying land-cover and indirect approaches such as estimating primary productivity (Turner et al., 2003). Both are fields of intense current research and both are influenced by irradiance effects which are inevitable in high resolution data. Despite a clear demand, there have been few studies employing strictly physical methods in order to compensate such effects. This thesis provides novel insights on this topic and is a useful reference for researchers considering similar approaches. As demonstrated, determination of irradiance and reflectances at TOC level relies on high quality auxiliary data. This emphasizes the value of LiDAR data availability. It must be precisely georeferenced and have a high point-density as it is a requirement for both high resolution DOMs and voxel grids. 3D canopy radiative transfer models such as DART show much potential as diverse products can be derived from them at each step of the simulation. The products used in this study can likely be optimized further to exploit the advantages of ray tracing through turbid voxel grids. As is, all TOC-based approaches show inherent issues which limit their applications. The retrieval of vegetation information is increasingly moving away from TOC to TOA. Pioneering work has been done by Laurent et al. (2011) on estimating vegetation properties from TOA radiances by performing forward simulations and minimizing cost functions. Further iterations of this approach can increase the number of free parameters by improved modelling of their probability distribution. In order to do this operationally and for large datasets, approximations of irradiance fractions as they are produced in this study could be integrated to reduce the parameter space. Solutions on how to identify and deal with underestimation of irradiance for steep slopes would first have to be found for DOM utilization, which is an interesting topic of potential further research based on this study.

A | MODTRAN Interrogation Technique

This appendix provides further details on the MODTRAN interrogation technique. The technique was developed by Verhoef & Bach (2003) as an efficient way of deriving the parameters necessary to describe radiative transfer through the atmosphere. Only three MODTRAN runs are performed for a uniform Lambertian surface with albedos of 0%, 50% and 100%. All further parameters can be derived from the MODTRAN outputs PATH (total path radiance), GSUN (radiance contribution due to ground-reflected sunlight), and GTOT (total ground-reflected radiance contribution), as well as the extraterrestrial solar irradiance E_s^o (Verhoef & Bach, 2003; Damm et al., 2015b). GSUN for a 100% reflective surface is equal to direct irradiance E^{dir} if the sensor height is set to 0 m above ground. E^{dir} can also be described as

$$E^{dir} = \tau_{ss} \frac{E_s^o \cos\theta_s}{\pi} \tag{A.1}$$

From this we get τ_{ss} as

$$\tau_{ss} = \frac{E^{dir}\pi}{E_s^o \cos\theta_s} \tag{A.2}$$

The remaining unknowns ρ_{dd}, τ_{sd} and τ_{do} can then be determined by the following equations:

$$\rho_{dd} = \frac{GTOT_{100} - 2 * GTOT_{50}}{GTOT_{100} - GTOT_{50}} \tag{A.3}$$

$$\tau_{sd} = [GTOT_{100}(1 - \rho_{dd})/GSUN_{100} - 1]\tau_{ss} \tag{A.4}$$

$$\tau_{do} = \frac{PATH_{100} - PATH_0}{GTOT_{100}} \tau_{oo} \tag{A.5}$$

These parameters vary depending on atmospheric state and geometric configuration. In this study they are determined for five different ground heights and interpolated but variations of viewing geometry are not considered.

B | Radiative Transfer

This appendix provides details and illustrations concerning the radiative transfer through the atmosphere. The study describes radiative transfer by way of the four-stream theory and the fluxes involved are illustrated in fig. (B.1). The components of irradiance on the target as well as the composition of radiance at sensor are shown alongside the atmospheric transfer functions influencing the flux (for description see section 2.3.1.1). An example of transfer function LUT values before convolution is given in fig. (B.2) (see tab. (2.1) for T-function reference). Here the complex absorption features of O_2 and H_2O are distinctly visible. Fig. (B.3) displays the solar irradiance on a flat surface at TOA ($T_1 * \pi$). Surface irradiance spectra and at-sensor radiance spectra can be obtained by combining T_1 with transfer functions T_{2-11} as described by the formulas in section 2.3.1.1. Fluxes which were not considered in this study are omitted, such as fluorescence, ground and atmosphere emitted thermal radiance as well as terrain reflected irradiance. These fluxes would ideally be included in a more sophisticated radiative transfer model but for many applications they are not essential.

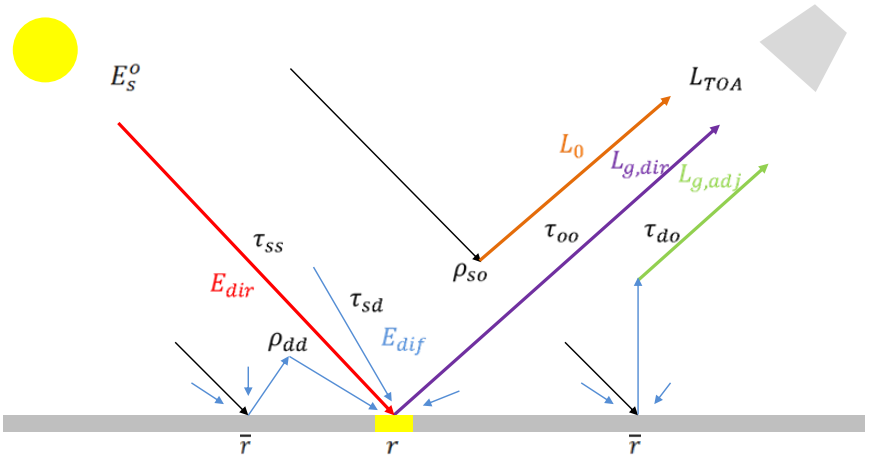

Figure B.1.: Illustration of the radiative transfer through the atmosphere. The main radiative fluxes are separated by colour. Red: Direct irradiance on target, blue: Diffuse irradiance on target, purple: Target reflected radiance at sensor, orange: Path scattered radiance at sensor, green: Background reflected radiance at sensor.

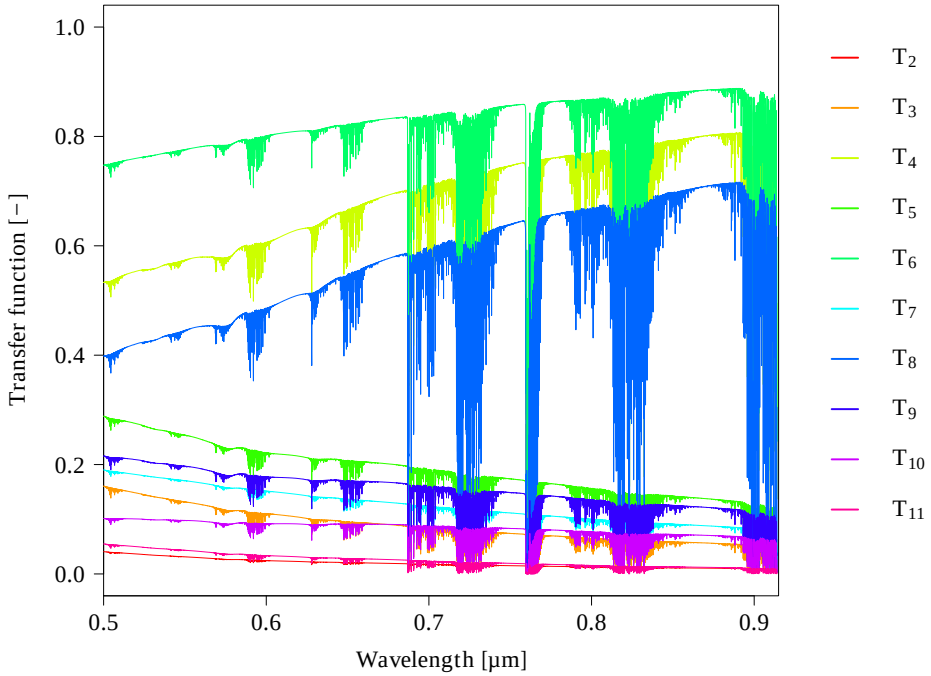

Figure B.2.: MODTRAN5 simulated atmospheric transfer functions for the wavelengths of interest as used in this study (depicted for 26.06.2010, 15:30 UTC, 600m a.s.l.).

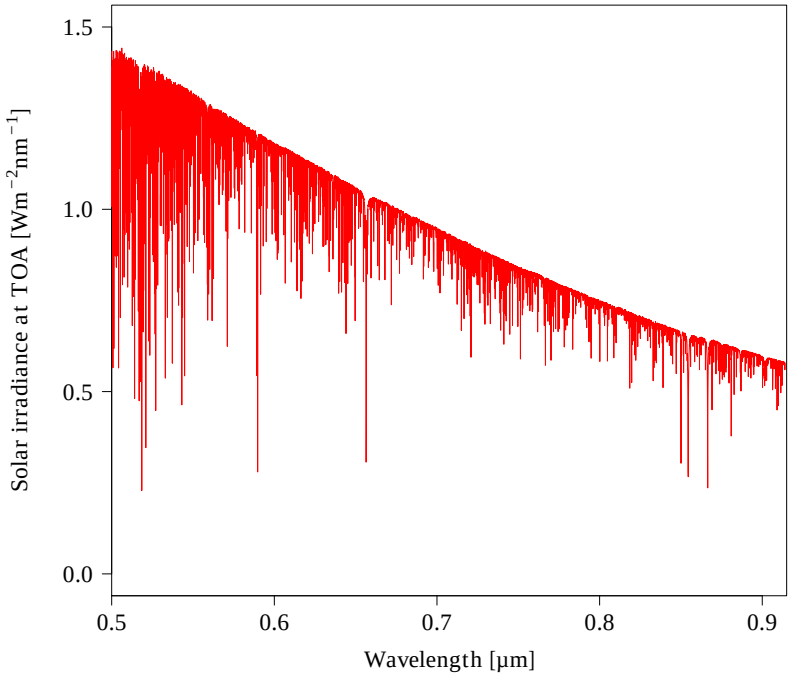

Figure B.3.: MODTRAN5 simulated solar irradiance at TOA (depicted for 26.06.2010, 15:30 UTC).

C | Pseudo-Invariant Surfaces

This appendix contains images of the pseudo-invariant surfaces used to evaluate the performance of the simple DEM approach in comparison with ATCOR-4. As ground-truth, two ASD field spectroradiometer (ASD FieldSpec, Analytical Spectral Devices, USA) measurements acquired during the 2010 APEX validation campaign in Wettingen, Switzerland were used. The surfaces are yellow tartan of the Wettingen sports-ground (47°28'02.30"N 8°18'33.90"E) and a black roof of the swimming baths (47°27'58.84"N 8°18'38.86"E), depicted in fig. (C.1). The measurements were conducted close to acquisition time for both dates.

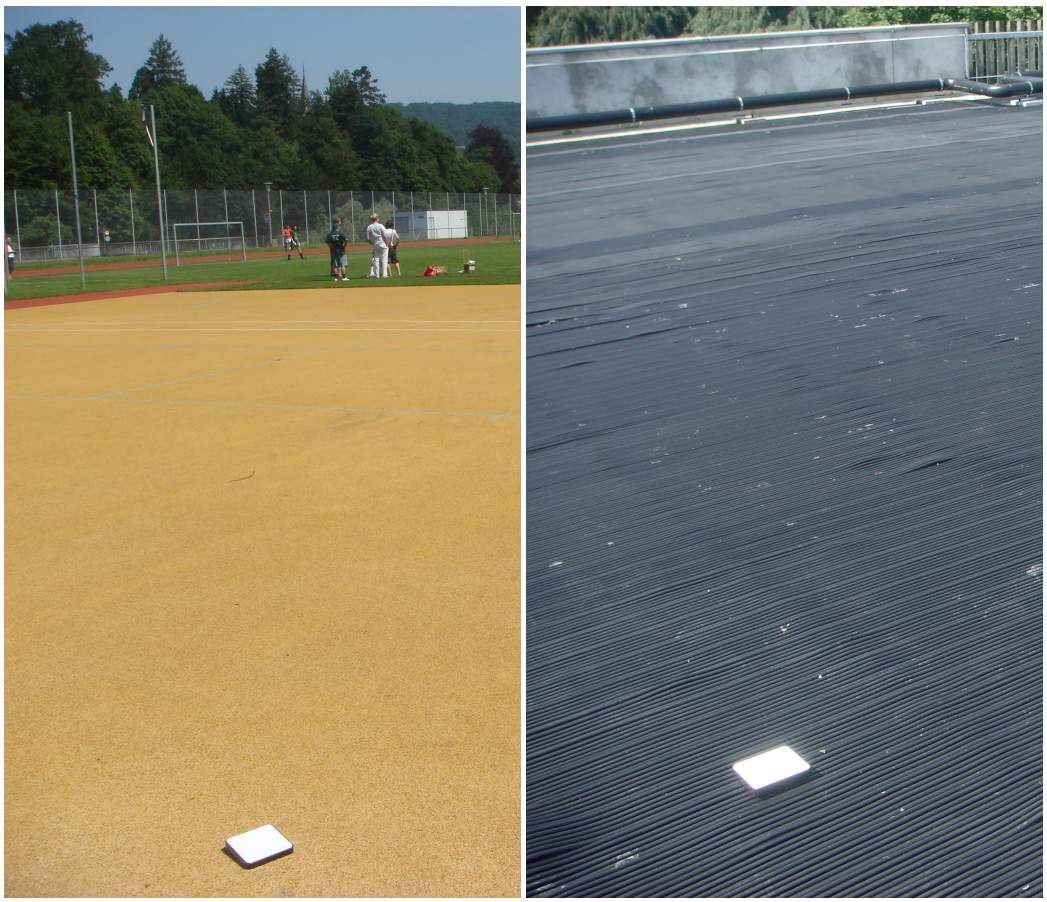

Figure C.1.: Images showing the yellow tartan (left) and dark roof (right) pseudo-invariant surfaces with a Spectralon white-reference panel. (Photos: M. Kneubühler, UZH).

D | RGB HCRF Composites

This appendix includes RGB composites of the HCRF results showing the extent of the scene covered by all auxiliary data. Fig. (D.1) displays the result of the smoothed DEM approach while fig. (D.2) and fig. (D.3) respectively show the DOM and DART approach results. The overcorrections over the forest for the DOM approach are clearly visible as well as consistently improved cast-shadow HCRF for both DOM and DART approaches. The blue shift towards the edge of the flight strip, which is visible in all results but accentuated in corrected cast-shadows, already appears in the radiance data and is likely due to view angle dependent scattering effects.

Figure D.1.: RGB composite (red: 640 nm, green: 553 nm, blue: 472 nm) of HCRF data for the 26th of June 2010 at 15:30 UTC, resulting from the DEM approach.

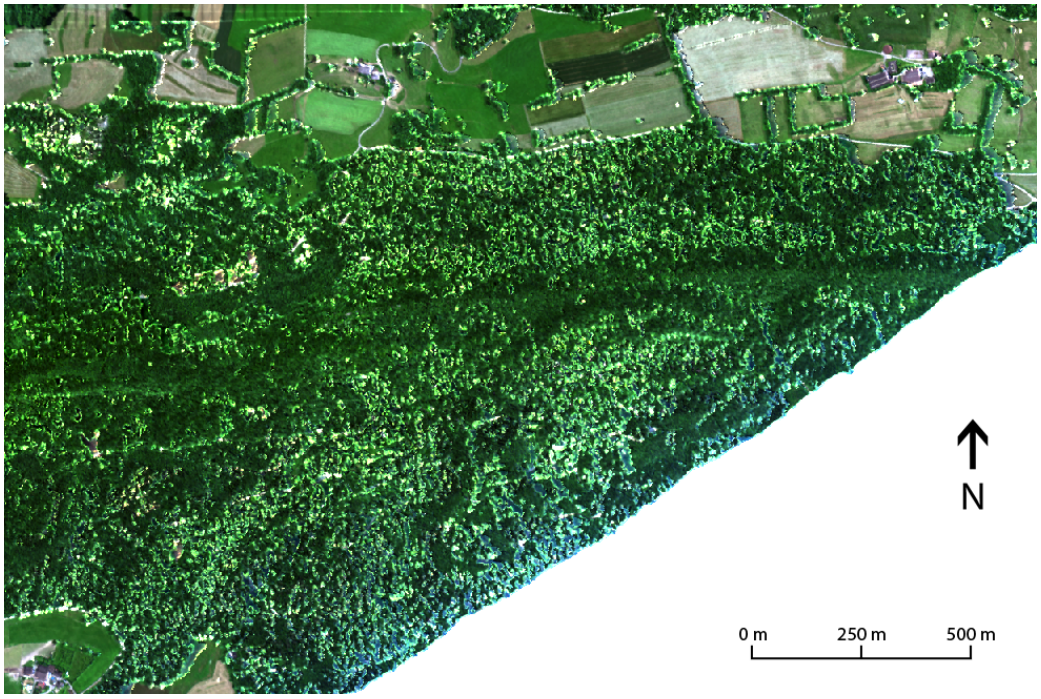

Figure D.2.: RGB composite (red: 640 nm, green: 553 nm, blue: 472 nm) of HCRF data for the 26th of June 2010 at 15:30 UTC, resulting from the DOM approach.

Figure D.3.: RGB composite (red: 640 nm, green: 553 nm, blue: 472 nm) of HCRF data for the 26th of June 2010 at 15:30 UTC, resulting from the DART approach.

E | DART Derived Irradiance Fraction Maps

This appendix includes example images of the DART derived scaling factors for direct (fig. E.1) and diffuse (fig. E.2) irradiance.

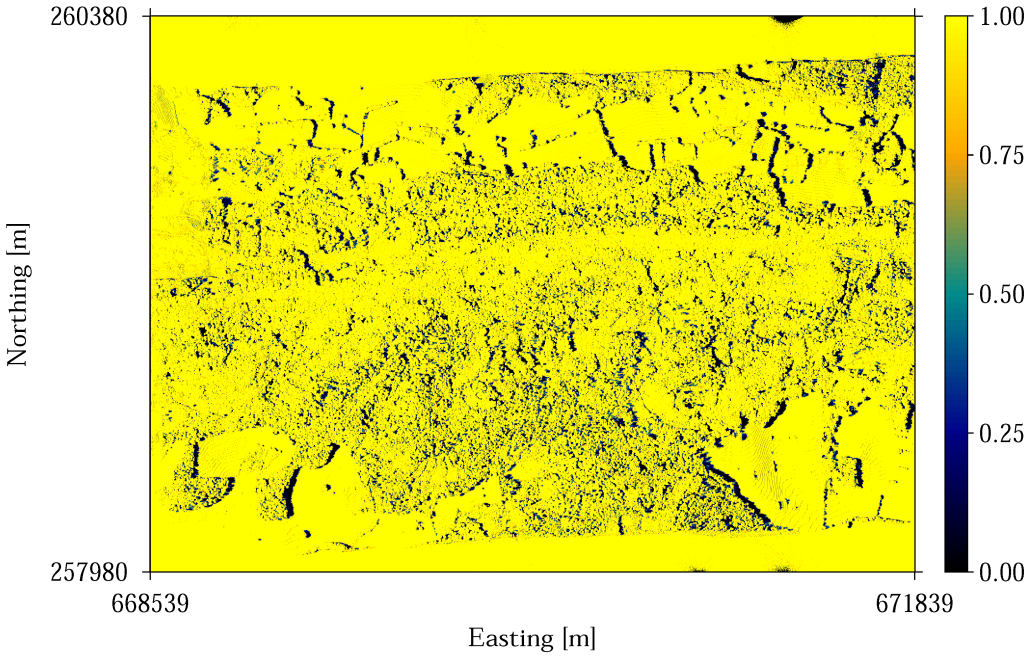

Figure E.1.: DART simulation based scaling factors for direct irradiance at 552.6 nm (Laegern, 26.06.2010, 15:30 UTC). Coordinates: CH1903 / LV03 (irradiance data courtesy of F. D. Schneider, UZH).

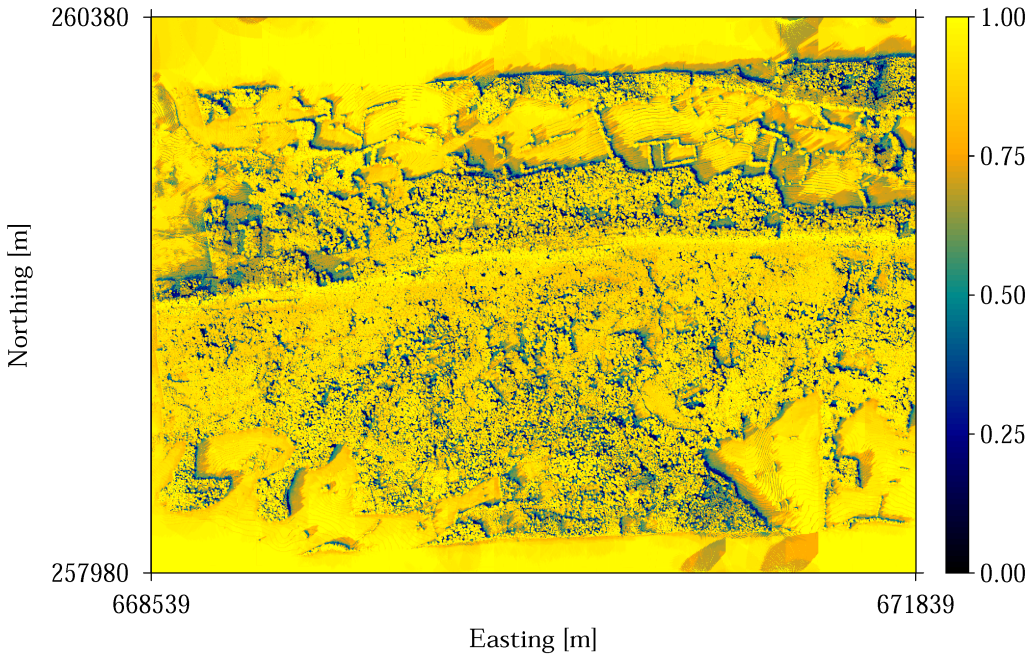

Figure E.2.: DART simulation based scaling factors for diffuse irradiance at 552.6 nm (Laegern, 26.06.2010, 15:30 UTC). Coordinates: CH1903 / LV03 (irradiance data courtesy of F. D. Schneider, UZH).

F | Vegetation Index Results

This appendix includes maps showing the calculated indices for the full scene extent covered by all auxiliary data and for all approaches. Depicted are the NDVI (fig. F.1), the PRI (fig. F.2), CHL (fig. F.3) and CAR (fig. F.4) results.

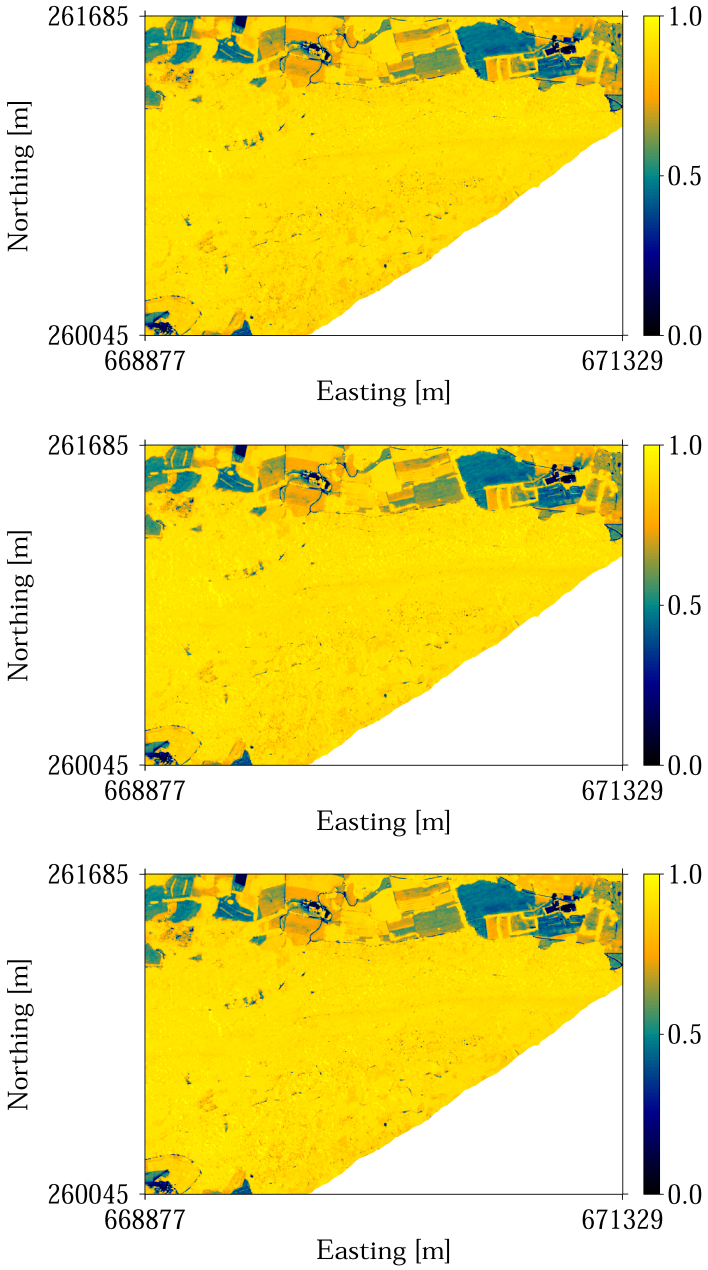

Figure F.1.: NDVI values for the 26th of June 2010 at 15:30 UTC, resulting from the DEM (top), DOM (middle) and DART (bottom) approaches. Coordinates: CH1903 / LV03.

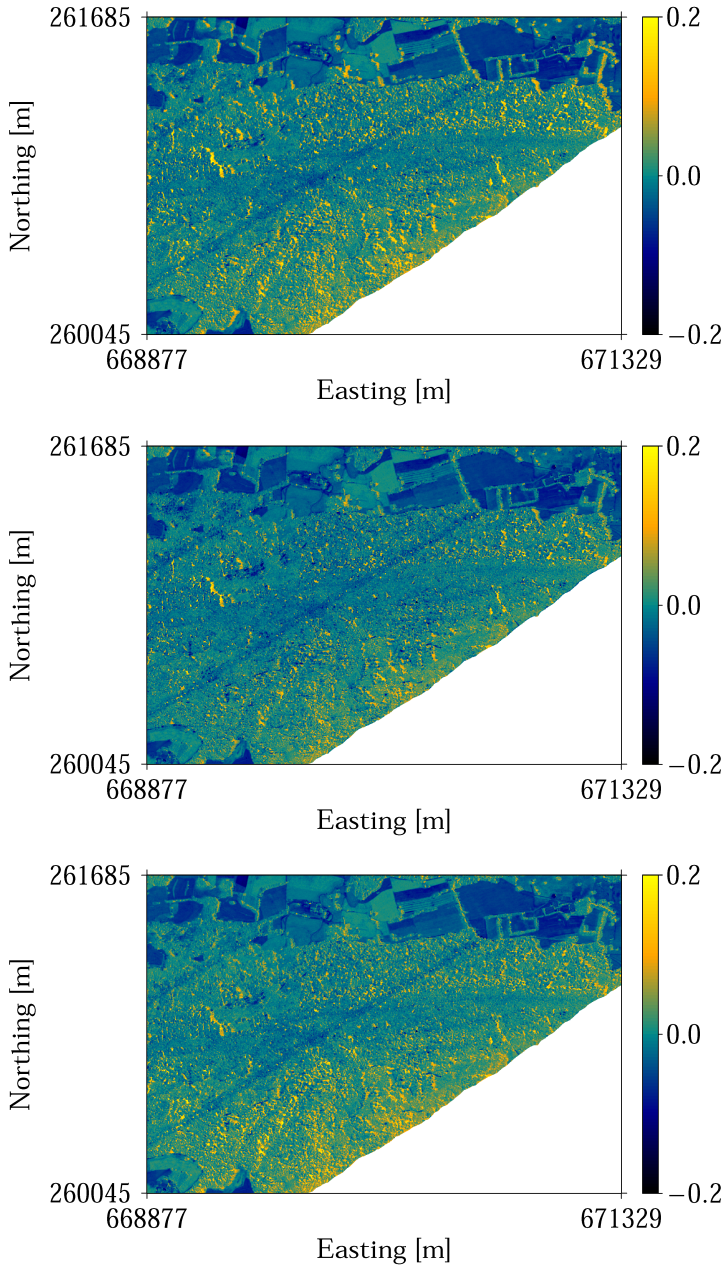

Figure F.2.: PRI values for the 26th of June 2010 at 15:30 UTC, resulting from the DEM (top), DOM (middle) and DART (bottom) approaches. Coordinates: CH1903 / LV03.

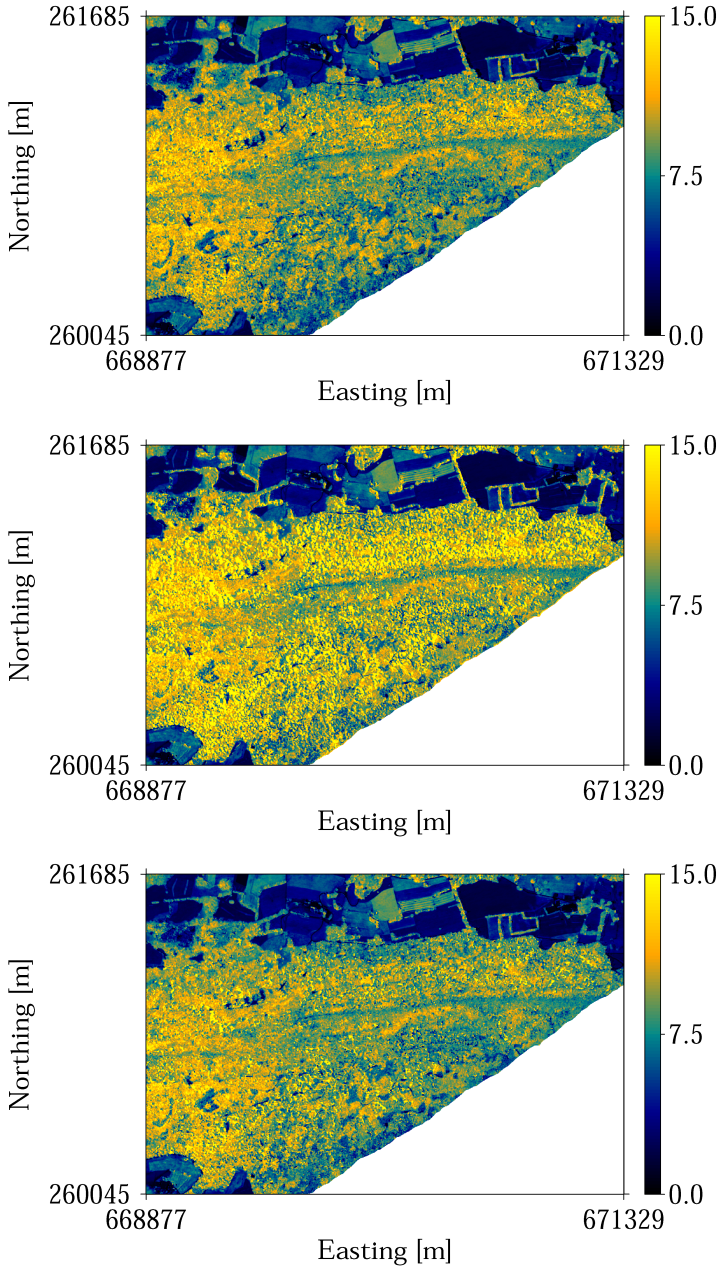

Figure F.3.: CHL values for the 26th of June 2010 at 15:30 UTC, resulting from the DEM (top), DOM (middle) and DART (bottom) approaches. Coordinates: CH1903 / LV03.

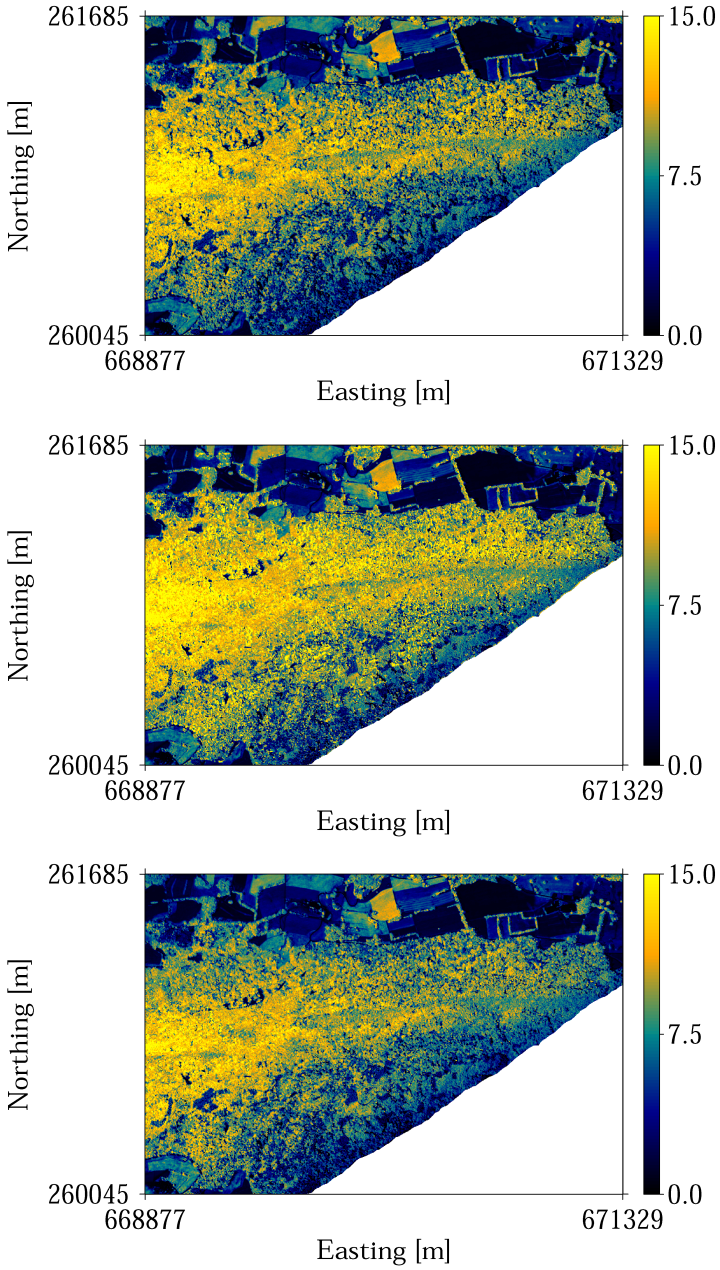

Figure F.4.: CAR values for the 26th of June 2010 at 15:30 UTC, resulting from the DEM (top), DOM (middle) and DART (bottom) approaches. Coordinates: CH1903 / LV03.

References

Adler-Golden, S. M., Matthew, M. W., Anderson, G. P., Felde, G. W., & Gardner, J. A. (2002). Algorithm for de-shadowing spectral imagery. *Proc. SPIE*, *4816*, 203–210.

Baldocchi, D., Falge, E., Gu, L. H., Olson, R., Hollinger, D., Running, S., Anthoni, P., Bernhofer, C., Davis, K., Evans, R., Fuentes, J., Goldstein, A., Katul, G., Law, B., Lee, X. H., Malhi, Y., Meyers, T., Munger, W., Oechel, W., Paw, K. T., Pilegaard, K., Schmid, H. P., Valentini, R., Verma, S., Vesala, T., Wilson, K., & Wofsy, S. (2001). FLUXNET: A new tool to study the temporal and spatial variability of ecosystem-scale carbon dioxide, water vapor, and energy flux densities. *Bulletin of the American Meteorological Society*, *82*, 2415–2434.

Berk, A., Anderson, G. P., Acharya, P. K., Bernstein, L. S., Muratov, L., Lee, J., Fox, M., Adler-Golden, S. M., Chetwynd Jr., J. H., Hoke, M. L., Lockwood, R. B., Gardner, J. A., Cooley, T. W., Borel, C. C., Lewis, P. E., & Shettle, E. P. (2006). MODTRAN5: 2006 update. *Proc. SPIE*, *6233*, 62331F.

Berk, A., Bernstein, L. S., & Robertson, D. C. (1989). *MODTRAN: A moderate resolution model for LOWTRAN 7*. Technical Report Geophys. Lab Bedford, MA, USA.

Berni, J. A. J., Zarco-Tejada, P. J., Suárez, L., & Fereres, E. (2009). Thermal and narrowband multispectral remote sensing for vegetation monitoring from an unmanned aerial vehicle. *IEEE Transactions on Geoscience and Remote Sensing*, *47*, 722–738.

Brunner, P., Hendricks Franssen, H. J., Kgotlhang, L., Bauer-Gottwein, P., & Kinzelbach, W. (2007). How can remote sensing contribute in groundwater modeling? *Hydrogeology Journal*, *15*, 5–18.

Cho, H. K., Jeong, M. J., Kim, J., & Kim, Y. J. (2003). Dependence of diffuse photosynthetically active solar irradiance on total optical depth. *Journal of Geophysical Research: Atmospheres*, *108*, 4267.

Cleland, E. E., Chuine, I., Menzel, A., Mooney, H. A., & Schwartz, M. D. (2007). Shifting plant phenology in response to global change. *Trends in Ecology and Evolution*, *22*, 357–365.

Cogliati, S., Verhoef, W., Kraft, S., Sabater, N., Alonso, L., Vicent, J., Moreno, J., Drusch, M., & Colombo, R. (2015). Remote Sensing of Environment Retrieval of sun-induced fluorescence using advanced spectral fitting methods. *Remote Sensing of Environment*, *169*, 344–357.

Combal, B., Baret, F., Weiss, M., Trubuil, A., Macé, D., Pragnère, A., Myneni, R., Knyazikhin, Y., & Wang, L. (2003). Retrieval of canopy biophysical variables from bidirectional reflectance using prior information to solve the ill-posed inverse problem. *Remote Sensing of Environment*, *84*, 1–15.

Conel, J. E., Green, R. O., Vane, G., Bruegge, C. J., Alley, R. E., & Curtiss, B. J. (1987). AIS-2 radiometry and a comparison of methods for the recovery of ground reflectance. In G. Vane (Ed.), *Proceedings of the 3rd Airborne Imaging Spectrometer Data Analysis Workshop* (pp. 18–47). Pasadena, CA, USA.

Cox, P., Betts, R., Jones, C., Spall, S., & Totterdell, I. (2000). Acceleration of global warming due to carbon-cycle feedbacks in a coupled climate model. *Nature*, *408*, 184–187.

Damm, A., Elber, J., Erler, A., Gioli, B., Hamdi, K., Hutjes, R., Kosvancova, M., Meroni, M., Miglietta, F., Moersch, A., Moreno, J., Schickling, A., Sonnenschein, R., Udelhoven, T., Van der Linden, S., Hostert, P., & Rascher, U. (2010). Remote sensing of sun-induced fluorescence to improve modeling of diurnal courses of gross primary production (GPP). *Global Change Biology*, *16*, 171–186.

Damm, A., Guanter, L., Paul-Limoges, E., Van der Tol, C., Hueni, A., Buchmann, N., Eugster, W., Ammann, C., & Schaepman, M. E. (2015a). Far-red sun-induced chlorophyll fluorescence shows ecosystem-specific relationships to gross primary production: An assessment based on observational and modeling approaches. *Remote Sensing of Environment*, *166*, 91–105.

Damm, A., Guanter, L., Verhoef, W., Schläpfer, D., Garbari, S., & Schaepman, M. E. (2015b). Impact of varying irradiance on vegetation indices and chlorophyll fluorescence derived from spectroscopy data. *Remote Sensing of Environment*, *156*, 202–215.

Drusch, M., Moreno, J., Del Bello, U., Franco, R., Golas, Y., Huth, A., Kraft, S., Middleton, E., Miglietta, F., Mohammed, G., Nedbal, L., Rascher, U., Schüttenmeyer, D., & Verhoef, W. (2016). The Fluorescence Explorer (FLEX) Mission Concept ESA's Earth Explorer 8 (EE8). *IEEE Transactions on Geoscience and Remote Sensing*, (p. tbd).

Eugster, W., Zeyer, K., Zeeman, M., Michna, P., Zingg, A., Buchmann, N., & Emmenegger, L. (2007). Methodical study of nitrous oxide eddy covariance measurements using quantum cascade laser spectrometery over a Swiss forest. *Biogeosciences*, *4*, 927–939.

Gamon, J. A., & Bond, B. (2013). Effects of irradiance and photosynthetic downregulation on the photochemical reflectance index in Douglas-fir and ponderosa pine. *Remote Sensing of Environment*, *135*, 141–149.

Gamon, J. A., Peñuelas, J., & Field, C. (1992). A narrow-waveband spectral index that tracks diurnal changes in photosynthetic efficiency. *Remote Sensing of Environment*, *41*, 35–44.

Gamon, J. A., Serrano, L., & Surfus, J. S. (1997). The photochemical reflectance index: An optical indicator of photosynthetic radiation use efficiency across species, functional types, and nutrient levels. *Oecologia*, *112*, 492–501.

Gao, B. C., Montes, M. J., Davis, C. O., & Goetz, A. F. H. (2009). Atmospheric correction algorithms for hyperspectral remote sensing data of land and ocean. *Remote Sensing of Environment*, *113*, S17–S24.

Gastellu-Etchegorry, J.-P., Demarez, V., Pinel, V., & Zagolski, F. (1996). Modeling radiative transfer in heterogeneous 3-D vegetation canopies. *Remote Sensing of Environment*, *58*, 131–156.

Gastellu-Etchegorry, J.-P., Guillevic, P., Zagolski, F., Demarez, V., Trichon, V., Deering, D., & Leroy, M. (1999). Modeling BRF and radiation regime of boreal and tropical forests. *Remote Sensing of Environment*, *68*, 281–316.

Gastellu-Etchegorry, J.-P., Yin, T., Lauret, N., Cajgfinger, T., Gregoire, T., Grau, E., Feret, J.-b., Guilleux, J., Cook, B. D., Morton, D., Rubio, J., Durrieu, S., Cazanave, G., Martin, E., Ristorcelli, T., & Thenkabail, P. S. (2015). Discrete anisotropic radiative transfer (DART 5) for modelling airborne and satellite spectroradiometer and LIDAR acquisitions of natural and urban landscapes. *Remote Sensing*, *7*, 1667–1701.

Gifford, R. (1994). The global carbon cycle: A viewpoint on the missing sink. *Australian Journal of Plant Physiology*, *21*, 1–15.

Gilks, W. R., Richardson, S., & Spiegelhalter, D. J. (1996). *Markov chain Monte Carlo in practice* volume 1. London: Chapman and Hall.

Gitelson, A. A., Keydan, G. P., & Merzlyak, M. N. (2006). Three-band model for noninvasive estimation of chlorophyll, carotenoids, and anthocyanin contents in higher plant leaves. *Geophysical Research Letters*, *33*, 2–6.

Hall, F. G., Hilker, T., Coops, N. C., Lyapustin, A., Huemmrich, K. F., Middleton, E., Margolis, H., Drolet, G., & Black, T. A. (2008). Multi-angle remote sensing of forest light use efficiency by observing PRI variation with canopy shadow fraction. *Remote Sensing of Environment*, *112*, 3201–3211.

Hay, J. E., & McKay, D. C. (1985). Estimating solar irradiance on inclined surfaces: A review and assessment of methodologies. *International Journal of Solar Energy*, *3*, 203–240.

Holben, B. N., Eck, T. F., Slutsker, I., Tanré, D., Buis, J. P., Setzer, A., Vermote, E., Reagan, J. A., Kaufman, Y. J., Nakajima, T., Lavenu, F., Jankowiak, I., & Smirnov, A. (1998). AERONETA Federated Instrument Network and Data Archive for Aerosol Characterization. *Remote Sensing of Environment*, *66*, 1–16.

Hueni, A., Biesemans, J., Meuleman, K., Dell'Endice, F., Schläpfer, D., Odermatt, D., Kneubühler, M., Adriaensen, S., Kempenaers, S., Nieke, J., & Itten, K. I. (2009). Structure, components, and interfaces of the airborne prism experiment (APEX) processing and archiving facility. *IEEE Transactions on Geoscience and Remote Sensing*, *47*, 29–43.

Itten, K. I., & Meyer, P. (1993). Geometric and radiometric correction of TM data of mountainous forested areas. *IEEE Transactions on Geoscience and Remote Sensing*, *31*, 764–770.

Kobayashi, S., & Sanga-Ngoie, K. (2008). The integrated radiometric correction of optical remote sensing imageries. *International Journal of Remote Sensing*, *29*, 5957–5985.

Kruse, F. A. (1988). Use of airborne imaging spectrometer data to map minerals associated with hydrothermally altered rocks in the northern grapevine mountains, Nevada, and California. *Remote Sensing of Environment*, *24*, 31–51.

Kustas, W. P., & Norman, J. M. (1996). Use of remote sensing for evapotranspiration monitoring over land surfaces. *Hydrological Sciences Journal*, *41*, 495–516.

Launay, M., & Guerif, M. (2005). Assimilating remote sensing data into a crop model to improve predictive

performance for spatial applications. *Agriculture, Ecosystems and Environment*, *111*, 321–339.

Laurent, V. C., Schaepman, M. E., Verhoef, W., Weyermann, J., & Chávez, R. O. (2014). Bayesian object-based estimation of LAI and chlorophyll from a simulated Sentinel-2 top-of-atmosphere radiance image. *Remote Sensing of Environment*, *140*, 318–329.

Laurent, V. C., Verhoef, W., Clevers, J. G., & Schaepman, M. E. (2011). Estimating forest variables from top-of-atmosphere radiance satellite measurements using coupled radiative transfer models. *Remote Sensing of Environment*, *115*, 1043–1052.

Malenovský, Z., Bartholomeus, H. M., Acerbi-Junior, F. W., Schopfer, J. T., Painter, T. H., Epema, G. F., & Bregt, A. K. (2007). Scaling dimensions in spectroscopy of soil and vegetation. *International Journal of Applied Earth Observation and Geoinformation*, *9*, 137–164.

Malenovský, Z., Homolová, L., Zurita-Milla, R., Lukeš, P., Kaplan, V., Hanuš, J., Gastellu-Etchegorry, J. P., & Schaepman, M. E. (2013). Retrieval of spruce leaf chlorophyll content from airborne image data using continuum removal and radiative transfer. *Remote Sensing of Environment*, *131*, 85–102.

McVicar, T. R., & Jupp, D. L. (1998). The current and potential operational uses of remote sensing to aid decisions on drought exceptional circumstances in Australia: a review. *Agricultural Systems*, *57*, 399–468.

Mõttus, M., Takala, T. L., Stenberg, P., Knyazikhin, Y., Yang, B., & Nilson, T. (2015). Diffuse sky radiation influences the relationship between canopy PRI and shadow fraction. *ISPRS Journal of Photogrammetry and Remote Sensing*, *105*, 54–60.

Mousivand, A., Verhoef, W., Menenti, M., & Gorte, B. (2015). Modeling top of atmosphere radiance over heterogeneous non-Lambertian rugged terrain. *Remote Sensing*, *7*, 8019–8044.

Nemani, R., Keeling, C., Hashimoto, H., Jolly, W., Piper, S., Tucker, C., Myneni, R., & Running, S. (2003). Climate-driven increases in global terrestrial net primary production from 1982 to 1999. *Science*, *300*, 1560–1563.

Ouaidrari, H., & Vermote, E. F. (1999). Operational atmospheric correction of Landsat TM data. *Remote Sensing of Environment*, *70*, 4–15.

Porcar-Castell, A., Tyystjärvi, E., Atherton, J., Van der Tol, C., Flexas, J., Pfündel, E. E., Moreno, J., Frankenberg, C., & Berry, J. A. (2014). Linking chlorophyll a fluorescence to photosynthesis for remote sensing applications: Mechanisms and challenges. *Journal of Experimental Botany*, *65*, 4065–4095.

Riaño, D., Chuvieco, E., Salas, J., & Aguado, I. (2003). Assesment of different topographic corrections in Landsat -TM data for mapping vegetation types. *IEEE Transactions on Geoscience and Remote Sensing*, *41*, 1056–1061.

Richter, R. (1990). A fast atmospheric correction algorithm applied to Landsat TM images. *International Journal of Remote Sensing*, *11*, 159–166.

Richter, R. (1998). Correction of satellite imagery over mountainous terrain. *Applied Optics*, *37*, 4004–4015.

Richter, R., Kellenberger, T., & Kaufmann, H. (2009). Comparison of topographic correction methods. *Remote Sensing*, *1*, 184–196.

Richter, R., & Schläpfer, D. (2002). Geo-atmospheric processing of airborne imaging spectrometry data. Part 2: Atmospheric/ topographic correction. *International Journal of Remote Sensing*, *23*, 2631–2649.

Richter, R., & Schläpfer, D. (2016). *ATCOR-4 User Guide* volume 7.0.3.

Richter, R., Schläpfer, D., & Müller, A. (2011). Operational atmospheric correction for imaging spectrometers accounting for the smile effect. *IEEE Transactions on Geoscience and Remote Sensing*, *49*, 1772–1780.

Roberts, D. A., Yamaguchi, Y., & Lyon, R. J. P. (1986). Comparison of various techniques for calibration of AIS data. In *Proceedings of the 2nd Airborne Imaging Spectrometer Data Analysis Workshop* (pp. 21–30). Pasadena, CA, USA.

Rodell, M., Houser, P. R., Jambor, U., Gottschalck, J., Mitchell, K., Meng, C.-J., Arsenault, K., Cosgrove, B., Radakovich, J., Bosilovich, M., Entin, J. K., Walker, J. P., Lohmann, D., & Toll, D. (2004). The Global Land Data Assimilation System. *Bull. Am. Meteorol. Soc.*, *85*, 381–394.

Sandmeier, S., & Itten, K. I. (1997). A physically-based model to correct atmospheric and illumination effects in optical satellite data of rugged terrain. *IEEE Transactions on Geoscience and Remote Sensing*, *35*, 708–717.

Schaepman, M. E., Jehle, M., Hueni, A., D'Odorico, P., Damma, A., Weyermann, J., Schneider, F. D., Laurent, V., Popp, C., Seidel, F. C., Lenhard, K., Gege, P., Küchler, C., Brazile, J., Kohler, P., De Vos, L., Meuleman, K., Meynart, R., Schläpfer, D., Kneubühler, M., & Itten, K. I. (2015). Advanced ra-

diometry measurements and Earth science applications with the Airborne Prism Experiment (APEX). *Remote Sensing of Environment*, *158*, 207–219.

Schaepman-Strub, G., Schaepman, M. E., Painter, T. H., Dangel, S., & Martonchik, J. V. (2006). Reflectance quantities in optical remote sensing-definitions and case studies. *Remote Sensing of Environment*, *103*, 27–42.

Schimel, D. (1995). Terrestrial ecosystems and the carbon cycle. *Global change biology*, *1*, 77–91.

Schläpfer, D., Koetz, B., Gruber, S., & Morsdorf, F. (2003). The influence of DEM characteristics on preprocessing of DAIS / ROSIS data in high altitude alpine terrain. In *3rd EARSeL workshop on imaging spectroscopy* (pp. 13–16). Herrsching, Germany.

Schläpfer, D., & Richter, R. (2002). Geo-atmospheric processing of airborne imaging spectrometry data. Part 1: Parametric orthorectification. *International Journal of Remote Sensing*, *23*, 2609–2630.

Schläpfer, D., Richter, R., & Damm, A. (2013). Correction of shadowing in imaging spectroscopy data by quantification of the proportion of diffuse illumination. In *8th SIG-IS EARSeL Imaging Spectroscopy Workshop*. Nantes, France.

Schneider, F. D., Leiterer, R., Morsdorf, F., Gastellu-Etchegorry, J. P., Lauret, N., Pfeifer, N., & Schaepman, M. E. (2014). Simulating imaging spectrometer data: 3D forest modeling based on LiDAR and in situ data. *Remote Sensing of Environment*, *152*, 235–250.

Schneider, F. D., Leiterer, R., Schaepman, M. E., & Morsdorf, F. (2015). Canopy height and plant area index changes in a temperate forest between 2010 2014 using airborne laser scanning. In S. Durrieu, & C. Véga (Eds.), *Proceedings of SilviLaser 2015, 14th conference on Lidar Applications for Assessing and Managing Forest Ecosystems*. La Grande Motte, France.

Schröter, D., Cramer, W., Leemans, R., Prentice, I., Araujo, M., Arnell, N., Bondeau, A., Bugmann, H., Carter, T., Gracia, C., de la Vega-Leinert, A., Erhard, M., Ewert, F., Glendining, M., House, J., Kankaanpaa, S., Klein, R., Lavorel, S., Lindner, M., Metzger, M., Meyer, J., Mitchell, T., Reginster, I., Rounsevell, M., Sabate, S., Sitch, S., Smith, B., Smith, J., Smith, P., Sykes, M., Thonicke, K., Thuiller, W., Tuck, G., Zaehle, S., & Zierl, B. (2005). Ecosystem service supply and vulnerability to global change in Europe. *Science*, *310*, 1333–1337.

Sitch, S., Huntingford, C., Gedney, N., Levy, P. E., Lomas, M., Piao, S. L., Betts, R., Ciais, P., Cox, P., Friedlingstein, P., Jones, C. D., Prentice, I. C., & Woodward, F. I. (2008). Evaluation of the terrestrial carbon cycle, future plant geography and climate-carbon cycle feedbacks using five Dynamic Global Vegetation Models (DGVMs). *Global Change Biology*, *14*, 2015–2039.

Takala, T. L., & Mõttus, M. (2016). Spatial variation of canopy PRI with shadow fraction caused by leaf-level irradiation conditions. *Remote Sensing of Environment*, *182*, 99–112.

Teillet, P. M., Guindon, B., & Goodenough, D. G. (1982). On the slope-aspect correction of multispectral scanner data. *Canadian Journal of Remote Sensing*, *8*, 84–106.

Tilling, A. K., O'Leary, G. J., Ferwerda, J. G., Jones, S. D., Fitzgerald, G. J., Rodriguez, D., & Belford, R. (2007). Remote sensing of nitrogen and water stress in wheat. *Field Crops Research*, *104*, 77–85.

Tucker, C. J. (1979). Red and photographic infrared linear combinations for monitoring vegetation. *Remote Sensing of Environment*, *8*, 127–150.

Turner, D. P., Urbanski, S., Bremer, D., Wofsy, S. C., Meyers, T., Gower, S. T., & Gregory, M. (2003). A cross-biome comparison of daily light use effciency for gross primary production. *Global Change Biology*, *9*, 383–395.

Van der Tol, C., Verhoef, W., Timmermans, J., Verhoef, A., & Su, Z. (2009). An integrated model of soil-canopy spectral radiances, photosynthesis, fluorescence, temperature and energy balance. *Biogeosciences*, *6*, 3109–3129.

Verhoef, W., & Bach, H. (2003). Simulation of hyperspectral and directional radiance images using coupled biophysical and atmospheric radiative transfer models. *Remote Sensing of Environment*, *87*, 23–41.

Verhoef, W., & Bach, H. (2007). Coupled soil-leaf-canopy and atmosphere radiative transfer modeling to simulate hyperspectral multi-angular surface reflectance and TOA radiance data. *Remote Sensing of Environment*, *109*, 166–182.

Verhoef, W., & Bach, H. (2012). Simulation of Sentinel-3 images by four-stream surface-atmosphere radiative transfer modeling in the optical and thermal domains. *Remote Sensing of Environment*, *120*, 197–207.

Verhoef, W., Van der Tol, C., & Middleton, E. M. (2014). Vegetation canopy fluorescence and reflectance retrieval by model inversion using optimization. In *5th International Workshop on Remote Sensing of Vegetation Fluorescence* (pp. 759–770). Paris, France.

Yin, T., Gastellu-Etchegorry, J. P., Lauret, N., Grau, E., & Rubio, J. (2013). A new approach of direction discretization and oversampling for 3D anisotropic radiative transfer modeling. *Remote Sensing of Environment*, *135*, 213–223.

Acknowledgements

First and foremost I would like to thank my supervisor Alex who always had time to discuss any issues and provided very helpful inputs throughout my thesis. I thank Fabian for his great scientific assistance and for providing the LaTEX template, as well as Daniel K. for the interesting discussions and crucial insights. I am also grateful for the expert advice on atmospheric correction by Daniel S. Further, Andy and Hendrik were very helpful in explaining the nuances of APEX data processing. I would like to especially thank my co-authors Wouter, Daniel S., Fabian, Michael and Alex whose suggestions helped improve the paper. Last but not least, a big thank you goes to all of my family and friends, especially my fellow students Moritz and Basil for their advice and company throughout the creation of this thesis.

Personal Declaration

I hereby declare that the submitted thesis is the result of my own, independent, work. All external sources are explicitly acknowledged in the thesis.

Place, Date Signature